CNWRA–2012–001

POTENTIAL RELEASES INSIDE A SPENT NUCLEAR FUEL DRY STORAGE CASK DUE TO IMPACTS: RELEVANT INFORMATION AND DATA NEEDS

Prepared for

U.S. Nuclear Regulatory Commission
Contract NRC–02–07–006

Prepared by

Roland Benke[1]
Hundal Jung[1]
Amitava Ghosh[1]
Yi-Ming Pan[1]
John C. Tait[2]

[1]Center for Nuclear Waste Regulatory Analyses
San Antonio, Texas

[2]Tait Consulting (2006) Inc.
Pinawa, Manitoba, Canada

August 2012

CONTENTS

FIGURES

TABLES

EXECUTIVE SUMMARY

The technical bases are being evaluated for regulating spent nuclear fuel (SNF) storage beyond 120 years. A literature survey was performed to support technical bases for potential releases of radioactive material from damaged fuel contained within a dry storage cask. The scope of work was limited to the assessment of factors and parameters pertaining to the releases from SNF rods within a canister of a dry storage cask.

Parameter definitions and the organizational framework for this report are based on NUREG–1864 (NRC, 2007) to evaluate the fraction of SNF that may be released from a hypothetical drop of a transportation cask (Chapter 1). Parameter values were selected based on an assessment of available data (Chapter 2). The assessment addressed the response of fuel rod cladding to impacts (Chapter 3), fuel pellet response to impacts (Chapter 4), and aerosol dynamics of fission gas and entrained particulate flow from breached SNF rods into the canister (Chapter 5). Areas in which further detailed technical investigations could significantly reduce uncertainties in the overall source term were identified (Chapter 6). Source term considerations for canister and cask breaches as well as the release of radioactive material into the atmosphere and environment were not investigated because they were beyond the scope of this project.

The assessment considered four representative SNF types: boiling water reactor SNF with burnup between 45 and 62.5 GWd/MTU (high burnup); pressurized water reactor SNF with high burnup; boiling water reactor SNF with burnup less than 45 GWd/MTU (low burnup); and pressurized water reactor SNF with low burnup. Compared to the values in NUREG–1864 (NRC, 2007) for high-burnup boiling water reactor SNF, available literature information supported lower parameter values for a few parameters, such as (i) $F_{init,body}$—the mass fraction of UO_2 in the body of SNF in a rod that has been converted to respirable fuel fines by abrasion and vibration before the impact, (ii) A—the area of the flow path within a rod, and (iii) F_{bed}—the fraction of respirable particles not captured during flow through a particle bed. For a few other parameters, differences in values between NUREG–1864 (NRC, 2007) and available literature data were small. In some cases, no additional information was found in the literature to support an alternative parameter value or range. Quantitative information on parameter values for high-burnup boiling water reactor SNF is provided in Table 2-1. Parameter values and knowledge gaps were also assessed for the other three representative SNF types. Quantitative parameter information for these other SNF types is provided in Table 2-2.

Reference

NRC. NUREG–1864, "A Pilot Probabilistic Risk Assessment of a Dry Cask Storage System at a Nuclear Power Plant." Washington, DC: U.S. Nuclear Regulatory Commission. March 2007.

ACKNOWLEDGMENTS

This report was prepared to document work performed by the Center for Nuclear Waste Regulatory Analyses (CNWRA®) for the U.S. Nuclear Regulatory Commission (NRC) under Contract No. NRC–02–007–006. The studies and analyses reported here were performed on behalf of the NRC Office of Nuclear Regulatory Research. The report is an independent product of CNWRA and does not necessarily reflect the views or regulatory position of NRC.

The authors wish to thank X. He for her technical review, G. Wittmeyer for his programmatic and editorial reviews, and B. Street for her administrative support in the report preparation.

QUALITY OF DATA, ANALYSES, AND CODE DEVELOPMENT

DATA: All CNWRA-generated original data contained in this report meet the quality assurance requirements described in the Geosciences and Engineering Division Quality Assurance Manual. Sources for other data should be consulted for determining the level of quality for those data.

ANALYSES AND CODES: No scientific or engineering software was used in the analyses contained in this report.

1 INTRODUCTION

NUREG–1864 (NRC, 2007, Appendix D) describes a model to evaluate the fraction of spent nuclear fuel (SNF) present inside a transportation cask that may be released in a hypothetical drop of the cask from different heights. It also provides details of the parameters representing response of the fuel rods and their cladding as well as flow of gases and particulates out of the rods. NUREG–1864 (NRC, 2007, Appendix D) reports data limitations and uncertainties in several areas. In this project, an assessment of new and existing information was performed to support evaluation of the technical basis for regulating SNF storage beyond 120 years. Staff surveyed existing information from the literature on the factors that influence the release fractions of radioactive material from SNF, recommend parameter values, present rationale for parameter value selection, and identified areas for further research to reduce uncertainties. Assumptions and certain other aspects are highlighted in the following list:

- Canister breach was assumed not to occur, and helium fill gas pressure inside the cask was assumed to be 0.1 to 0.5 MPa [1 to 5 atm].

- Assessment focused on Zircaloy cladding, Zircaloy-2 for boiling water reactors (BWRs) and Zircaloy-4 for pressurized water reactors (PWRs). Alternative cladding alloys, such as Zirlo™ and M5™, were not considered.

- Initial oxide thickness on cladding was considered to be the same as that at the time of removal from the reactor. Additional oxidation from incomplete drying or external air was not considered during extended storage, due to the explicit assumption that the canister does not breach.

- The assessment considered four representative SNF types:

  — PWR with burnup less than 45 GWd/MTU
  — PWR with burnup between 45 and 62.5 GWd/MTU
  — BWR with burnup less than 45 GWd/MTU
  — BWR with burnup between 45 and 62.5 GWd/MTU

  These lower and higher levels for pellet-average burnup are referred to in this report simply as “low” and “high” burnup, respectively.

- A range of impact loads was considered from transportation vibrations, seismic loads, and equivalent drop heights from 1 to 9 m [3 to 30 ft]. Selection of parameter values focused on an equivalent drop height of 9 m [30 ft].

Certain aspects explicitly not considered are:

- Damage and degradation to the concrete overpack and canister.

- Spallation of Chalk River Unidentified Deposits (CRUD), or corrosion products on outer cladding and assembly surfaces, and its potential source term contribution.

- Influences from thermal shock during drying.

- Fire and external thermal challenges.

The assessment and parameter value selection in this report align with the U.S. Nuclear Regulatory Commission (NRC) methodology for the source term determination (NRC, 2007). Chapter 2 elaborates upon this relationship. Assessment of literature data and selection of parameter values for the source term determination are organized into three chapters. Fuel rod response to impact loads is presented in Chapter 3. Fuel pellet response is addressed in Chapter 4. Aerosol dynamics considerations are discussed in Chapter 5.

2 SOURCE TERM DETERMINATION METHODOLOGY AND PARAMETER VALUES

A cask drop during transportation of SNF may generate impact forces that are severe enough to breach the cladding and fuel rods. Some fraction of available material within failed fuel rods could be released to the environment outside of the cask. The release fraction, both as particles and fission gases, from the cask, F_{rel}, is [NRC, 2007, Appendix D, Eq. (D.1)]

$$F_{rel} = F_{rods} \cdot F_{RC} \cdot F_{CE} \tag{2-1}$$

where, F_{rods} is the fraction of the fuel rods in each assembly that fail in the cask, F_{RC} is the fraction of available material released from the rods to the cask environment, and F_{CE} is the part (or fraction) of F_{RC} that is transported through the breach to the environment outside of the cask. Assessments in this report focus on releases into the canister. Releases from the canister or cask and to the environment are not included in this report. Source terms from fuel fines and release of fission gases are considered for further assessment. Although spallation of solid Chalk River Unidentified Deposits (CRUD) or corrosion products on the cladding surface can contribute to the source term, their contribution was beyond the scope of this project and, therefore, was not considered in this assessment.

The number and size of breaches in a rod affect the release of fuel fines. NRC (2007, Appendix D) characterizes the number and size of breaches with three parameters: number of fracture locations along a rod $(n_{tears/rod})$, fracture length (l_c), and fracture width (w_c). Fractures formed in the cladding due to impact forces can lead to fuel pellet exposure and provide leak paths for fission gas and particulate releases. Depressurization of the fuel rods would allow fission gases and fuel fines to flow into the canister environment. Time needed for gas depressurization from a rod into the canister or cask is estimated in NRC [2007, Eq. (D.3)] for an assumed gas flow through an orifice with a cross-section area A.

The release fraction of fuel particles, $F_{rel,particles}$, factors into F_{RC} term in Eq. (2-1) and can be estimated using the following equation [NRC, 2007, Eq. (D.7)]

$$F_{rel,particles} = 0.113\left(F_{init,rim} + F_{imp,rim}\right)\left\{\left[n_{tears/rod}F_{tear,rim}\right] + \left[F_{ent,rim}(F_{bed})\right]\right\} + 0.887\left\{n_{tears/rod}\left(F_{init,body} + F_{imp,body}\right)(F_{bed})\right\} \tag{2-2}$$

with the following parameters:

$F_{init,body}$ = fraction of mass of UO_2 in the body of SNF in a rod that has been converted to respirable fuel fines by abrasion and vibration before the impact

$F_{init,rim}$ = fraction of mass of UO_2 in the rim layer of SNF in a rod that has been converted to respirable fuel fines by abrasion and vibration before the impact

$F_{imp,body}$ = fraction of mass of UO_2 in the body of spent fuel pellet that is converted to respirable fuel fines by brittle fracture due to the impact

$F_{imp,rim}$ = fraction of mass of UO_2 in the rim layer of a SNF pellet that is converted to respirable fuel fines by brittle fracture due to the impact

$F_{tear,rim}$ = fraction of mass of UO_2 in the rim layer that is blown out of the rod from one rod tear during rod depressurization without filtering by passage through a particle bed

$F_{ent,rim}$ = fraction of mass of UO_2 in the rim layer that is entrained in the depressurization gas flow through the rim layer-cladding gap and transported to the rod tear and then out into the cask

F_{bed} = fraction of respirable particles that are not captured during flow through a particle bed

The fraction of fission gas released from the rod after fracture to the cask, R_{RC_g}, also factors into the F_{RC} term in Eq. (2-1) and is defined by NRC (2007, p. D–14) as

$$R_{RC_g} = {}^{I_f}/_{I} \tag{2-3}$$

where I_f is the fission gas released and I is the total fission gas inventory.

The fraction of material in chemical group k that escapes from the cask to the outside environment leaving the rest within the cask is estimated using the following equation [NRC, 2007, Eq. (D.13)]

$$F_{CE,k} = \left[1 - F_{deposition,k}\right]\left[1 - \frac{P_{atm}}{P_{rod\ failure}}\right] \tag{2-4}$$

where

$F_{deposition,k}$ = fraction of materials in chemical element group k that is deposited onto cask interior surfaces after release to the cask atmosphere from failed rods

P_{atm} = atmospheric pressure

$P_{rod\ failure}$ = pressure that the depressurized cask would reach upon rod failure if release of rod gases to the environment were not occurring

The rest of the material in chemical element group k does not escape the cask. The P_{rod} parameter is defined as the pressure of He and fission product noble gases in a rod at ambient conditions released by pellet fracturing. As described by NRC (2007, p. D–16), P_{rod} factors into the calculation of $P_{rod\ failure}$. Although the release of material to the atmosphere and environment in Eq. (2-4) is not explicitly considered in this report, the P_{rod} and $F_{deposition,k}$ parameters are assessed in Sections 4.1.6 and 5.1.4, respectively, because they relate to releases of SNF into the canister, gas-borne suspension within the canister, and deposition within the canister. As described in NRC (2007, Section D.2.5), assessment of $F_{CE,k}$ includes consideration of the other parameters, such as the free volume within a spent fuel rod and number of moles of helium and fission product noble gases in a spent fuel rod. Detailed investigation into these other parameters was beyond the scope of this project.

Source term parameters addressed in this report are displayed in Figure 2-1. Compared to the total surface area of the cladding, anticipated breach sizes and number of breach sites are small. Accordingly, pathways for the flow of gas and particulates out of SNF rods are confined,

and aerosol dynamics must be considered to estimate the extent to which SNF particulates, generated within the fuel rod cladding, can be released from the fuel rods into the canister. The response of fuel rods and cladding to impact loads is captured in Chapter 3. Fuel pellet response and aerosol dynamics considerations are addressed in Chapters 4 and 5, respectively. Assessments in this report focus on potential impacts and cladding breaches that are large enough for particulate release. Parameter values were selected based on the availability of supporting data in the literature. These selections are presented in Table 2-1 for BWR SNF with high burnup. Corresponding parameter values for low-burnup PWR and BWR SNF (less than 45 GWd/MTU) and for high-burnup PWR SNF are provided in Table 2-2. Chapters 3, 4, and 5 contain supporting information for the parameter value selections, such as summaries of literature data, discussions on data relevance, and comments on associated uncertainties. Areas needing further research are identified in Chapter 6.

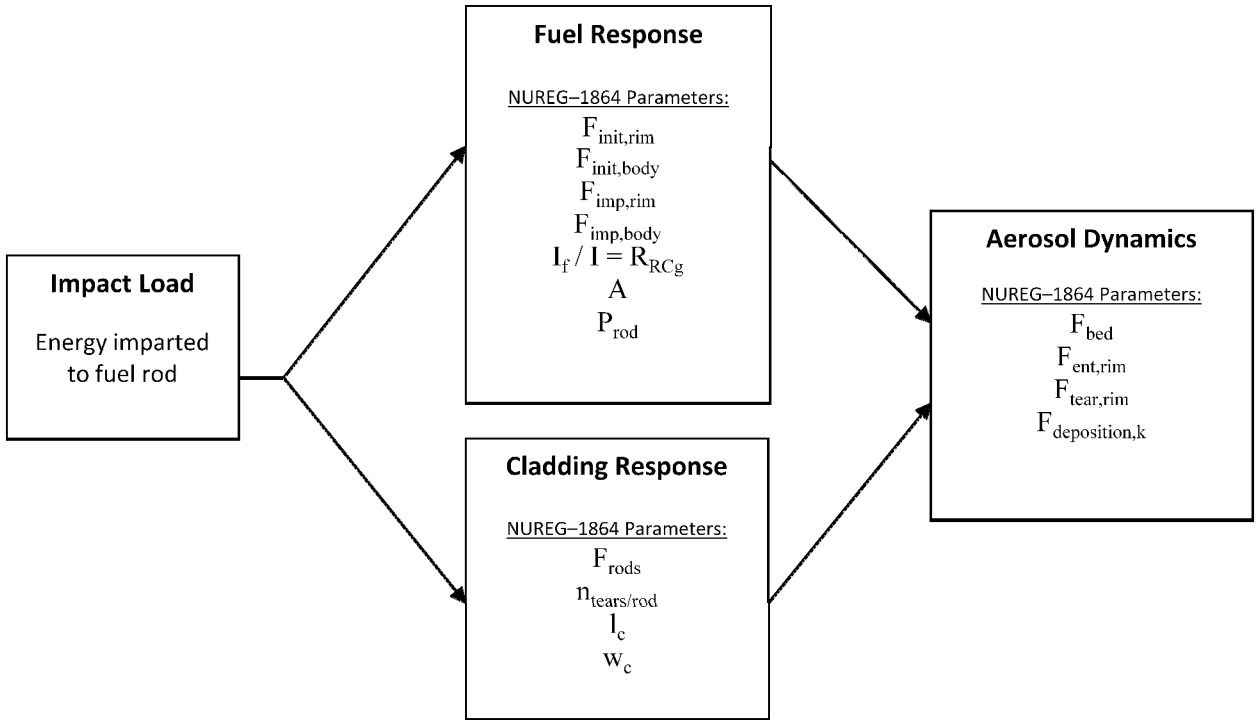

Figure 2-1. Flow Chart of Parameters for Estimating Potential Releases Inside a SNF Dry Storage Cask

Table 2-1. Suggested Parameter Values for High-Burnup (45–62.5 GWd/MTU) BWR Fuel			
NUREG–1864 (NRC, 2007)		Recommended Value(s)	Reference and Justification
Parameter	Value		
F_{rods}	0.33 to 1	No additional information found	This is an assumption in NUREG–1864 (NRC, 2007, p. D–21) for a 30.5-m [100-ft] drop. No additional information is available for a 9-m [30-ft] drop. Refer to Section 3.1.1.
$n_{tears/rod}$	5	No additional information found	This is an assumption in NUREG–1864 (NRC, 2007, p. D–8) for a 30.5-m [100-ft] drop. No additional information is available for a 9-m [30-ft] drop. Refer to Section 3.1.2.
l_c	17 mm [0.7 in]	No additional information found	Assigned in NUREG–1864 (NRC, 2007, p. D–4) for a 30.5-m [100-ft] drop, lack of data acknowledged. No additional information is available for a 9-m [30-ft] drop. Refer to Section 3.1.3.
w_c	1.7 mm [0.07 in]	No additional information found	Assigned in NUREG–1864 (NRC, 2007, p. D–4) for a 30.5-m [100-ft] drop, lack of data acknowledged. No additional information is available for a 9-m [30-ft] drop. Refer to Section 3.1.3.
$F_{init,body}$	2.4×10^{-5}	9×10^{-7} to 1.6×10^{-5}	Assessment of new data: Hanson, et al. (2008) estimated the fraction release for BWR SNF with a burnup of 53–69 GWd/MTU. Refer to Section 4.1.1.
$F_{init,rim}$	0 Reported in Einziger (2007)	No additional information found	No additional information is available. Refer to Section 4.1.2.
$F_{imp,body}$	4×10^{-5} Reported in Einziger (2007)	No additional information found	Einziger (2007) value corresponds to a 9-m [30-ft] drop. No additional information is available for a 9-m [30-ft] drop. Refer to Section 4.1.3.
$F_{imp,rim}$	4×10^{-5} to 1	No additional information found	NUREG–1864 (NRC, 2007, p. D–11) acknowledged that an uncertainty of several orders of magnitude exists in parameter value estimates. A range was assumed for $F_{imp,rim}$ in which the low value equaled the same fraction as the body. Complete fracture of the rim was assumed for the high value of the range. No additional information is available for a 9-m [30-ft] drop. Refer to Section 4.1.4.
R_{RCg}	0.12 to 0.4 [12 to 40%] (NRC, 2007)	0.05 to 0.15 [5 to 15%] from gap plus potential 0.03 to 0.3 [3 to 30%] from grain boundary for severe impact and pellet fracturing	Assessment of new data: In the absence of fission gas releases due to drop impacts, data from reactivity-initiated accident transient tests were reviewed and factored into suggested contributions due to severe impact and pellet fracturing. Refer to Section 4.1.5.
P_{rod}	~5 MPa [50 atm] (NRC, 2007)	2 MPa [20 atm] to 7.14 MPa [70 atm]	Assessment of new data: refer to Section 4.1.6 for additional information.

Table 2-1. Suggested Parameter Values for High-Burnup (45–62.5 GWd/MTU) BWR Fuel (continued)			
NUREG–1864 (NRC, 2007)		Recommended Value(s)	Reference and Justification
Parameter	Value		
A (cm^2)	9.6×10^{-6} assuming 35-µm hydraulic diameter and gap does not open (NRC, 2007)	0 to 7.1×10^{-6}	Assessment of existing information: refer to Table 4-6 in Section 4.1.7.
F_{bed}	0.1 [Inferred from equation at bottom of p. D–9 in NRC (2007) with L = 10ℓ]	0.015 to 0.03	Assessment of new and existing information: Leak path plugging considered due to smaller gap for higher burnup SNF. Values were determined for a gap width of 25 µm by applying particulate flow and plugging experimental results from Sutter, et al. (1980) to the anticipated flow geometry within SNF rods. Refer to Section 5.1.1 for additional information.
$F_{tear,rim}$	2.8×10^{-4}	No additional information found	Limited discussion provided in Section 5.1.2.
$F_{ent,rim}$	1	0.1 to 1	Considering limited existing information, a value of 0.1 is selected to define the low end of the recommended $F_{ent,rim}$ parameter range. No literature data were found to substantiate a different parameter range. Refer to Section 5.1.3 for additional information.
$F_{deposition,k}$	0.9 selected from range of 0.9 to 0.984 (NRC, 2007)	0.70 to 0.98	Assessment of existing information: The 0.98 value relates to a fractional deposition of 0.02 for a cask leak area of 3-mm^2 and slow depressurization. The 0.70 value relates to a fractional deposition of 0.3 for cask leak area of 100-mm^2 and rapid depressurization. Refer to Section 5.1.4 for additional information.

BWR = Boiling Water Reactor
LWR = Light Water Reactor
SNF = Spent Nuclear Fuel

Einziger, R.E. "Source Terms for Spent Fuel Transportation and Storage Cask Evaluation." Proceedings of the 15th International Symposium on the Packaging and Transportation of Radioactive Materials (PATRAM 2007), Miami, Florida, October 21–26, 2007. Deerfield, Illinois: Institute of Nuclear Materials Management. 2007.

Hanson, B.D., W. Wu, R.C. Daniel, P.J. MacFarlan, A.M. Casella, R.W. Shimskey, and R.S. Wittman. "Fuel-In-Air FY07 Summary Report." PNNL–17275, Rev. 1. Richland, Washington: Pacific Northwest National Laboratory. September 2008.

NRC. NUREG–1864, "A Pilot Probabilistic Risk Assessment of a Dry Cask Storage System at a Nuclear Power Plant." Washington DC: U.S. Nuclear Regulatory Commission. March 2007.

Sutter, S.L., J.W. Johnson, J. Mishima, P.C. Owzorski, L.C. Schwendiman, and G.B. Long. NUREG/CR–1099, "Depleted Uranium Dioxide Powder Flow Through Very Small Openings." ML20040901.0241. Washington, DC: U.S. Nuclear Regulatory Commission. February 1980.

Table 2-2. Suggested Parameter Values for PWR and BWR SNF With Low Burnup (Less Than 45 GWd/MTU) and PWR SNF With High Burnup (45–62.5 GWD/MTU)				
NUREG–1864 Parameter (NRC, 2007)	**Recommended Value(s)**			
	Low-Burnup PWR	**Low-Burnup BWR**	**High-Burnup PWR**	**Reference and Justification**
F_{rods}	0.004 to 0.04	0.0001 to 0.001	None	Assessment of existing information described in Section 3.1.1: Low-burnup PWR SNF Sanders, et al. (1992) estimated the maximum probability of a single rod breakage to be 5×10^{-5} for 21 15 × 15 PWR assemblies (total of 208 fuel rods in each assembly in the transportation cask) for a 9-m [30-ft] side drop of the cask. Maximum probabilities for longitudinal slit and formation of a pinhole in a rod are 2×10^{-5} and 2×10^{-4}, respectively, for same 9-m [30-ft] side drop. Therefore, expected number of failed fuel rods in each assembly varies from 0.004 ($2 \times 10^{-5} \times 208$) to 0.04 ($2 \times 10^{-4} \times 208$). Low-burnup BWR SNF Sanders, et al. (1992) estimated the maximum probability of a single rod breakage to be 2×10^{-6} for 52 7 × 7 BWR assemblies (total 48 fuel rods in each assembly in the transportation cask) for a 9-m [30-ft] corner drop of the cask. Maximum probabilities for longitudinal slit and formation of a pinhole in a rod are 2×10^{-5} and 8×10^{-6}, respectively, for a 9-m [30-ft] side drop and a 9-m [30-ft] corner drop, respectively. Therefore, expected number of failed rods in each assembly varies from 0.0001 ($2 \times 10^{-6} \times 48$) to 0.001 ($2 \times 10^{-5} \times 48$). High-burnup PWR SNF EPRI (2006a) estimated that 7 rods in each assembly of a 17 × 17 PWR transportation cask (2.5% or more) would experience a pinhole-size transverse (Mode I) failure in a 9-m [30-ft] drop. EPRI (2006a) also estimated that not more than 2.5% or 7 rods in each assembly would experience partial circumferential tear (Mode II) failure in such a drop. EPRI (2006b) estimated that 7 fuel rods in each assembly (~2.5%) would experience partial longitudinal hairline (Mode III) cracks of pinhole-size from a 9-m [30-ft] drop; however, only 0.005 rods per assembly will experience a complete through-wall longitudinal fracture. EPRI (2006a,b) applied a failure criterion using Critical Strain Energy Density. This failure criterion is not universally accepted as appropriate for estimating fuel rod failure from a drop. Consequently, no recommended value is provided. Refer to Section 3.2 for additional discussion.

Table 2-2. Suggested Parameter Values for PWR and BWR SNF With Low Burnup (Less Than 45 GWd/MTU) and PWR SNF With High Burnup (45–62.5 GWD/MTU) (continued)				
NUREG–1864 Parameter (NRC, 2007)	**Recommended Value(s)**			
	Low-Burnup PWR	**Low-Burnup BWR**	**High-Burnup PWR**	**Reference and Justification**
$n_{tears/rod}$	No additional information found	No additional information found	No additional information found	No additional information is available for a 9-m [30-ft] drop. Refer to Section 3.1.2.
l_c	No additional information found	No additional information found	No additional information found	EPRI (2006a) concluded that a full guillotine break of a fuel rod inside a transportation cask would not occur in a 9-m [30-ft] drop and estimated that partial Mode II tearing of 75% of the cross section would occur. As discussed in Section 3.2, the failure criterion used by EPRI is not universally acceptable. Consequently, the estimated value of tear size is not recommended. Limited discussion is given in Section 3.1.3.
w_c	No additional information found	No additional information found	No additional information found	EPRI (2006a) estimated 2-mm [0.08-in] opening at the widest point for a tear decreasing to zero at the root of the tear. As discussed, the failure criterion used by EPRI is not universally acceptable. Consequently, the estimated value of tear size is not recommended. Limited discussion is given in Section 3.1.3.
$F_{init,body}$	2.4×10^{-5}	2.4×10^{-5}	1×10^{-5} to 8×10^{-5}	Assessment of new data: Hanson, et al. (2008) estimated the fraction release for PWR SNF with a burnup of 45 GWd/MTU.
$F_{init,rim}$	Not applicable, no rim formation	Not applicable, no rim formation	No additional information found	No additional information is available for a 9-m [30-ft] drop. Refer to Section 4.1.2.
$F_{imp,body}$	No additional information found	No additional information found	No additional information found	No additional information is available for a 9-m [30-ft] drop. Refer to Section 4.1.3.
$F_{imp,rim}$	Not applicable, no rim formation	Not applicable, no rim formation	No additional information found	No additional information is available for a 9-m [30-ft] drop. Refer to Section 4.1.4.

Table 2-2. Suggested Parameter Values for PWR and BWR SNF With Low Burnup (Less Than 45 GWd/MTU) and PWR SNF With High Burnup (45–62.5 GWD/MTU) (continued)				
NUREG–1864 Parameter (NRC, 2007)	**Recommended Value(s)**			
	Low-Burnup PWR	**Low-Burnup BWR**	**High-Burnup PWR**	**Reference and Justification**
R_{RCg}	<1 to 5% release from gap plus potential for 3 to 20% release from grain boundary due to severe impact and pellet fracturing	<1 to 5% release from gap plus potential for 3 to 15% release from grain boundary due to severe impact and pellet fracturing	5 to 15% release from gap plus potential for 3 to 30% release from grain boundary due to severe impact and pellet fracturing	Assessment of new data: In the absence of information on fission gas releases due to drop impacts, data from reactivity-initiated accident transient tests were reviewed and factored into suggested contributions due to severe impact and pellet fracturing. Refer to Section 4.1.5.
P_{rod}	3 MPa [30 atm] (fill gas pressure) to 15.5 MPa [153 atm]	1 MPa [10 atm] (fill gas pressure) to 7.14 MPa [70 atm]	5 MPa [49 atm] to 15.5 MPa [153 atm]	Assessment of new data: Refer to Section 4.1.6 for additional information.
A (cm^2)	1.5×10^{-6}	No additional information found	0 to 7.9×10^{-7}	Assessment of existing information: Refer to Table 4-6 in Section 4.1.7.

Table 2-2. Suggested Parameter Values for PWR and BWR SNF With Low Burnup (Less Than 45 GWd/MTU) and PWR SNF With High Burnup (45–62.5 GWD/MTU) (continued)				
NUREG–1864 Parameter (NRC, 2007)	**Recommended Value(s)**			
	Low-Burnup PWR	**Low-Burnup BWR**	**High-Burnup PWR**	**Reference and Justification**
F_{bed}	0.003 to 0.007 for end breach, 0.005 to 0.010 for center breach	0.003 to 0.007 for end breach, 0.005 to 0.010 for center breach	0.01 due to leak path plugging	Assessment of new and existing information: Low-burnup PWR and BWR SNF No leak path plugging assumed due to larger gap for lower burnup SNF. Values were determined by applying measurement data from Otani, et al. (1989) to the anticipated flow geometry within SNF rods. Refer to Section 5.1.1 for additional information. High-burnup PWR SNF Leak path plugging considered due to smaller gap for higher burnup SNF. Values were determined by applying particulate flow and plugging experimental results from Sutter, et al. (1980) to the anticipated flow geometry within SNF rods. Compared to the value in Table 2-1 for BWR fuel at similar higher burnup, a lower value is recommended due to a smaller gap width reported in Table 4-6 for high-burnup PWR SNF. Refer to Section 5.1.1 for additional information.
$F_{tear,rim}$	Not applicable, no rim formation	Not applicable, no rim formation	No additional information found	No additional information was found in the literature for parameter value estimation. Refer to Section 5.1.2.
$F_{ent,rim}$	Not applicable, no rim formation	Not applicable, no rim formation	0.1 to 1	Considering limited existing information, a value of 0.1 is selected to define the low end of the recommended $F_{ent,rim}$ parameter range. No literature data were found to substantiate a different parameter range. Refer to Section 5.1.3 for additional information. NRC (2007, Section 2.4.1.3) recommends the high end value to be 1 unless information justifying smaller value is available.
$F_{deposition,k}$	0.70 to 0.98	0.70 to 0.98	0.70 to 0.98	Assessment of existing information: The 0.98 value relates to a fractional deposition of 0.02 for a cask leak area of 3-mm^2 and slow depressurization. The 0.70 value relates to a fractional deposition of 0.3 for cask leak area of 100-mm^2 and rapid depressurization. Refer to Section 5.1.4 for additional information.

Table 2-2. Suggested Parameter Values for PWR and BWR SNF With Low Burnup (Less Than 45 GWd/MTU) and PWR SNF With High Burnup (45–62.5 GWD/MTU) (continued)				
NUREG–1864 Parameter (NRC, 2007)	**Recommended Value(s)**			
	Low-Burnup PWR	**Low-Burnup BWR**	**High-Burnup PWR**	**Reference and Justification**
PWR = Pressurized Water Reactor SNF = Spent Nuclear Fuel BWR = Boiling Water Reactor LWR = Light Water Reactor				
EPRI. "Spent-Fuel Transportation Applications: Modeling of Spent-Fuel Rod Transverse Tearing and Rod Breakage Resulting from Transportation Accident." 1013447. Palo Alto, California: Electric Power Research Institute. 2006a.				
EPRI. "Spent Fuel Transportation Applications: Longitudinal Tearing Resulting from Transportation Accidents—A Probabilistic Treatment." 1013448. Palo Alto, California: Electric Power Research Institute. 2006b.				
Hanson, B.D., W. Wu, R.C. Daniel, P.J. MacFarlan, A.M. Casella, R.W. Shimskey, and R.S. Wittman. "Fuel-In-Air FY07 Summary Report." PNNL–17275, Rev. 1. Richland, Washington: Pacific Northwest National Laboratory. September 2008.				
NRC. NUREG–1864, "A Pilot Probabilistic Risk Assessment of a Dry Cask Storage System at a Nuclear Power Plant." Washington DC: U.S. Nuclear Regulatory Commission. March 2007.				
Otani, Y., C. Kanaoka, and H. Emi. "Experimental Study of Aerosol Filtration by the Granular Bed Over a Wide Range of Reynolds Numbers." *Aerosol Science and Technology*. Vol. 10. pp. 463–474. 1989.				
Sanders, T.L., K.D. Seager, Y.R. Rashid, P.R. Barrett, A.P. Malinauskas, R.E. Einziger, H. Jordan, T.A. Duffey, S.H. Sutherland, and P.C. Reardon. "A Method for Determining the Spent-Fuel Contribution to Transportation Cask Containment Requirements." SAND90–2406. Albuquerque, New Mexico: Sandia National Laboratories. November 1992.				
Sutter, S.L., J.W. Johnson, J. Mishima, P.C. Owzorski, L.C. Schwendiman, and G.B. Long. NUREG/CR–1099, "Depleted Uranium Dioxide Powder Flow Through Very Small Openings." ML20040901.0241. Washington, DC: U.S. Nuclear Regulatory Commission. February 1980.				

3 FUEL ROD RESPONSE ASSESSMENT

This chapter summarizes information available in the literature on the potential failure of spent fuel rods in hypothetical drop scenarios during transportation in approved transportation casks. Discussions include the impact loads assessed in different studies reported in the literature. Impact loads to fuel rods relate to impact loads of the surrounding canister. Fuel rod response is addressed following a brief introduction on canister impacts. As mentioned in the Introduction, canister failure is not investigated in this study.

Potential normal and accident scenarios associated with transportation of SNF canisters in transportation casks may induce impact loads on the SNF canisters. The mechanical loading environment of SNF during transportation is defined by 10 CFR Part 71. During normal transport conditions, the transportation cask would be subjected to shock and vibration normally applicable to rail and road transport in addition to the impact load from a cask drop of free fall of 0.3 m [1 ft] to a rigid target. Under hypothetical accident scenarios, the transportation cask would be subjected to an impact load from a drop onto a rigid target following a free fall of 9.0 m [30 ft] and onto a mild steel bar following a free fall of 1.0 m [3.3 ft].

The load transfer path from the cask to the fuel assemblies inside the cask depends strongly on cask drop orientation. Cask drops have been characterized in three possible orientations: (i) end drop, (ii) side drop, and (iii) corner drop (initial impact at an angle followed by slap down). In an end drop, the impact load transmits axially through each fuel rod from end plate to end plate. In a side drop, the load path is primarily through the basket to the spacer grids and end plates to the fuel rods. A corner drop can be viewed as a two-drop event; an initial impact of the cask at an angle followed by a slap down. Initial impact dominates when the impact angle is near vertical. In such a case, the response of the fuel assembly is similar to an end drop event. For cases with the impact angles near horizontal, the slap down phase dominates. The response of the fuel assembly resembles a side drop event.

Sanders, et al. (1992) described the shock and vibration imposed on SNF during transportation using both a truck-based and a rail-based transportation cask. The bounding acceleration response spectrum for the truck cask was based on actual measurements and can be described by a bilinear curve in a log-log scale: a linearly increasing portion up to a frequency of approximately 3.5 Hz, followed by a constant segment of 4.4g acceleration up to a maximum frequency of 300 Hz. As an alternative, a simplified boundary spectrum would be a straight line at 4.4g at frequencies up to 3.5 Hz. The rail-car coupling events are generally more severe than other rail car events that may generate a shock. Sanders, et al. (1992) provided the estimated acceleration from a 0.3-m [1-ft] drop of a lead-shielded truck cask with impact limiters in place onto an unyielding surface as a function of drop angle. For a 90° impact (end drop), acceleration during initial impact exceeded 100g but was small for other drop angles.

3.1 Existing Knowledge and Selection of Values for Fuel Rod Response to a Drop Event

Impact loads experienced by fuel rods in a drop event have been reported in a number of studies (e.g., Sanders, et al., 1992; EPRI, 2005a,b; 2006a,b; 2007; Wu, et al., 1991). All of these studies numerically simulated a drop event to estimate the impact load experienced by a fuel rod. The models used in the simulations conservatively assume that the cladding of a fuel rod provides the structural stiffness to tensile and bending loads because fuel pellets have a very low tensile strength [about 100 MPa (14,500 psi) for fuel pellets versus 690 MPa

(100,000 psi) for cladding (Sanders, et al., 1992)]. Thermal gradients in the fuel rods and creep of cladding can fracture the fuel pellets early in life (the first few irradiation cycles), which decreases the gap between the fuel pellets and cladding. Approximately 20 to 50 large fragments can develop (IAEA, 2011). Additional fractures may form in the irradiated fuel although neither the effects of burnup nor the differences between the BWR and PWR fuel on the fracture intensity have been systematically studied (IAEA, 2011). It is assumed in analyzing the end drop model that all rods in an assembly would be loaded simultaneously and equally. All rods would be in compression and would deform in the same pattern.

Low-Burnup Fuel

Sanders, et al. (1992) analyzed the impact on transportation casks loaded with BWR and PWR fuels with burnup less than 45 GWd/MTU from a 9-m [30-ft] drop with impact limiters in place. A cask can undergo an end drop, a side drop, or a corner drop. Analyses were conducted when no frictional force acting at the impact surface (100 percent slip) and with infinite friction (no slip). A fuel assembly may be damaged in three possible modes as a result of a drop during transportation (Sanders, et al., 1992; EPRI, 2007): (i) a transverse crack generally of pinhole size, Mode I; (ii) a guillotine break, Mode II; and (iii) an axial or a longitudinal split, Mode III. A transverse crack (Mode I failure) would result when the strain or elongation exceeds the material ductility limits. This mode of failure could occur in all types of impact conditions anticipated during transport but is most probable in side drop scenarios because plastic bending at the end plates dominates the response. The assumption is that a pellet-cladding interaction (PCI) crack would grow after initiation and would propagate through the wall forming a pinhole or a narrow crack in the cladding due to impact load from a drop event. A pinhole failure of a fuel rod could release fission gases and finely dispersed fuel (Sanders, et al., 1992). This transverse crack can extend through a large portion of the rod cross-section or even develop a guillotine break if additional energy is available (Mode II failure). This Mode II failure is controlled by the fracture toughness K_{IC} and is conditional to the Mode I failure (i.e., pinhole-size damage sites in the cladding that grow to guillotine breaks). A longitudinal crack can initiate at the inner surface of the fuel cladding from a PCI-induced crack or a manufacturing defect (Mode III failure). Assuming that PCI cracks are present, Sanders, et al. (1992), based on measurements, estimated that the maximum length of these PCI cracks would be approximately 28 percent of the cladding thickness. This mode of failure is dominant in side drop and corner drop (slap down phase) scenarios.

Fracture propagation is controlled by the stress intensity factor at the fracture tip (Sanders, et al., 1992). Sanders, et al. (1992) used the fracture toughness K_{IC} criterion to determine whether the fracture would grow under the loading conditions. A brittle oxide layer up to 100 μm thick may form at the outer cladding wall in addition to a hydride-rich sub-layer. The sub-layer may include both radial and circumferential hydride depending on the stress-temperature history during dry storage (EPRI, 2005a). Consequently, K_{IC} for Mode III failure could be different from K_{IC} for Mode II failure. Results of these analyses were compared with the material properties to determine whether cladding would fail. The material properties of cladding material (e.g., fracture toughness) can be expressed probabilistically. The probability of fracture of fuel rods can be estimated from the stress intensity factor and fracture toughness distributions.

For normal transportation scenarios (only random vibration and regulatory 0.3-m [1-ft] drop applicable), Sanders, et al. (1992) used material fracture criteria based on fatigue crack growth. For accidental drop scenarios, partial wall cracks resulting from fabrication defects form the initial crack distribution that grows to fracture the cladding. PCI occurs in the reactor when the

fuel pellets swell beyond the gap and produce small cracks in the cladding in the longitudinal direction. The best estimate of PCI is 75 cracks per rod for BWR and 60 for PWR SNF when removed from the reactor (Sanders, et al., 1992). Sanders, et al. (1992) noted that in-reactor damage has the highest potential to affect cladding integrity and performance during a transportation accident. During dry storage, fuel degradation mechanisms generally involve slow crack growth, which may eventually lead to a breach, but the probability of such a breach during dry storage was estimated by Sanders, et al. (1992) to be low. Following a drop during transportation, longitudinal cracks may propagate to develop longitudinal tears in the cladding. Circumferential cracks, such as manufacturing defects or pinholes created by material failure, may propagate under axial loads induced by bending. Circumferential cracks can become guillotine cracks, breaking the fuel rods into separate pieces during a sufficiently severe drop event.

High-Burnup Fuel

The Electric Power Research Institute (EPRI) (2005a,b; 2006a,b) analyzed the probability of failure of a high-burnup fuel rod as result of a 9-m [30-ft] drop during transportation. EPRI adopted the nomenclature of fuel rod failure modes (Mode I, II, or III failure) proposed by Sanders, et al. (1992) in their assessment. EPRI (2005a, 2007) showed that a 9-m [30-ft] drop of a cask with impact limiters can be replaced by a 9-m [30-ft] drop of a bare cask onto a concrete pad used in ISFSIs. The load, measured in terms of deceleration of the cask, in the equivalent case with bare casks, bounds the g-load with impact limiters onto an unyielding surface. Essentially, the concrete slab and subgrade act as the impact limiters by absorbing energy through concrete fracturing and crushing, and soil deformation (EPRI, 2005a). EPRI (2005a) developed a global structural model of a representative transportation cask using the ABAQUS explicit finite element program. An initial velocity of 13.4 m/s [43.9 ft/s] was specified for the model to represent a 9-m [30-ft] free-fall of the cask from rest in the horizontal position. The dynamic force parameters important to evaluation of failure of the fuel rods are pinch forces due to rod-to-rod impact, bending moments, and axial-extension and shear forces. Results of this analysis show significantly more plastic deformation of the basket structure at the bottom (impact side) of the cask than the basket structure near the top; however, these baskets did not collapse. The displacement estimated for a fuel assembly in a side drop is complex (EPRI, 2005a). This displacement is composed of vibration of individual fuel rods superimposed on the motion of the assembly acting as a composite beam. This motion is superimposed on the rigid body motion of the overall assembly. The rods are compacted in the vertical direction and impact the bottom and side plates of the baskets. The maximum pinch forces occur at the center spacer grid with a maximum of 33.8 kN [7,600 lb]. The computed pinch forces away from the center spacer grid are significantly smaller; more than 90 percent of the rods experience a pinch force less than half of this amount. The maximum pinch forces can be approximated by a normal distribution of 4.9 kN [1,100 lb]. The bundles near the bottom experience higher pinch forces than those at the top.

EPRI (2005a) also computed the axial force, shear force, and bending moment at the Center Spacer Grid and Top Plate sections (Table 3-1). The computed axial force, which is predominantly tensile, is less than 8 kN [1,800 lb] [approximately 90 MPa (13,000 psi) axial stress] at the Center Spacer Grid section. The largest shear force computed is less than 3.3 kN [750 lb] resulting in a maximum induced transverse shear stress less than 50 MPa [7,000 psi]. The maximum bending moment recorded is approximately 0.3 m-kN [300 in-lb], which produces a maximum bending stress of 100 MPa [15,000 psi]. The distribution of axial force, shear force, and bending moment can be approximated by a normal distribution. The stiff top-plate restricts

Table 3-1. Computed Parameters*							
	Maximum Pinch Force kN [lb]	Maximum Axial		Maximum Shear		Maximum Bending	
		Force kN [lb]	Stress MPa [psi]	Force kN [lb]	Stress MPa [psi]	Moment m-kN [in-lb]	Stress MPa [psi]
Center Spacer Grid Model	33.4 [7,500]	8.0 [1,800]	90 [13,000]	3.3 [750]	50 [7,000]	0.3 [300]	100 [15,000]
Top Plate Model	13.3 [3,000]	12.5 [2,800]	140 [21,000]	2.0 [450]	30 [4,350]	0.37 [370]	123 [17,800]
*EPRI. "Spent Fuel Transportation Applications: Global Forces Acting on Spent Fuel Rods and Deformation Patterns Resulting From Transportation Accident." EPRI–101817. Palo Alto, California: Electric Power Research Institute. 2005.							

displacement of the guide tubes but not the fuel rods. This results in substantial bending moment and shear deformation between the last spacer grid and the top plate (EPRI, 2005a). Maximum pinch force computed is 13.3 kN [3,000 lb], less than half of that computed in the Center Spacer Grid model. The recorded maximum axial force is 12.5 kN [2,800 lb], which translates to an axial stress of 140 MPa [21,000 psi]. This axial force is nearly twice the force for the Center Spacer Grid. Computed axial forces exhibit significant compressive and tensile nature with a long period flexural response. The maximum shear force is 2 kN [450 lb], substantially less than the shear force computed in the Center Spacer Grid model. The maximum bending moment is 0.37 m-kN [370 in-lb]. A normal distribution adequately approximates the pinch force, axial force, shear force, and bending moment variations computed.

Initiation of Mode I and propagating to develop Mode II failures depends mainly on the cladding hydride structure and gap between fuel and cladding. The fuel-clad gap controls the resistance to deformation. The hydride structure, primarily determined by the operational history of the fuel rods, affects the resistance to failure when subjected to impact loads. Initiation of Model I failure is affected by a corrosion (zirconium oxide) layer with maximum thickness of 100 μm and a thin (approximately 10 μm) layer of dense hydrides (hydride rim) having a hydrogen concentration in excess of 1,000 ppm (EPRI, 2006a). Once a Mode I failure is initiated at the outer diameter, the crack begins to grow into the cladding wall with increasing fracture resistance due to reduced hydride concentration until the crack front reaches the inner diameter (completion of Mode I failure). Thereafter, the crack grows circumferentially until a complete guillotine break develops (EPRI, 2006a).

3.1.1 Parameter F_{rods}

Values of the F_{rods} parameter reported in the literature are discussed in this section. NUREG–1864 (NRC, 2007) assumed that 0.33 to one rod in each assembly would fail in a 30.5 m [100 ft] drop of a HI-Storm 100 cask; however, no value for a 9 m [30 ft] drop has been reported. Additional information on F_{rods} has been identified in the literature for low burnup (less than 45 GWd/MTU) PWR and BWR fuels for a 9 m [30 ft] drop and is presented here and is also given in Table 2-2.

Low-Burnup Fuel

Sanders, et al. (1992) estimated the failure probability of both a PWR and a BWR rod from a 9-m [30-ft] drop under different modes. These values are given in Table 3-2. Knowing the failure probability of a single rod and the number of fuel rods in an assembly involved in a drop event, the values of F_{rods} have been calculated in this study. The estimated maximum failure probabilities of a PWR rod forming a pinhole crack and a longitudinal slit are approximately 2×10^{-4} per rod and 2×10^{-5} per rod in each drop, respectively. These failures of the fuel rods occurred in an end drop (slap down) and a side drop of a transportation cask from a height of 9 m [30 ft] (Sanders, et al., 1992). For a rail cask containing 21 15 × 15 PWR assemblies with 208 fuel bearing rods in each assembly in an event, estimated probabilities for a pinhole crack and a longitudinal slit formation in a drop are 0.04 [$2 \times 10^{-4} \times 208$] and 0.004 [$2 \times 10^{-5} \times 208$] per assembly, respectively. The estimated maximum failure probability of a rod breakage is approximately 5×10^{-5} per rod in a drop event and occurred in an end drop (slap down). Therefore, 0.01 [$5 \times 10^{-5} \times 208$] fuel rods are expected to break in each PWR assembly as a result of a 9-m [30-ft] drop during transportation.

Sanders, et al. (1992) also reported the estimated probabilities of fuel rod failures for a transportation cask containing 52 7 × 7 BWR assemblies (48 fuel rods per assembly). The maximum estimated probability of formation of pinhole cracks and longitudinal slits in a 9-m [30-ft] drop of a transportation cask are approximately 8×10^{-6} and 2×10^{-5} per rod per event. These probabilities are estimated during the initial impact phase of a corner drop and in a side drop of the cask, respectively (Sanders, et al., 1992). In other words, it is expected that 0.0004 [$8 \times 10^{-6} \times 48$] and 0.001 [$2 \times 10^{-5} \times 48$] rods in each assembly would develop a pinhole crack and a longitudinal slit, respectively, in a 9-m [30-ft] drop. The maximum estimated probability of a fuel rod breakage is 2×10^{-6} per rod during the initial phase of a corner drop, which translates to 0.0001 [$2 \times 10^{-6} \times 48$] rods breaking per assembly in a 9-m [30-ft] drop event.

Table 3-2. Estimated Failure Probability in Different Drop Scenarios Analyzed by Sandia National Laboratories in SAND90–2406*

Assembly Loading Conditions	Drop Angle	Failure Probability of Single Fuel Rod		
		Transverse Pinhole Rupture	Rod Breakage	Longitudinal Slit
7 × 7 BWR				
9-m End Drop	90	1×10^{-9}	2×10^{-13}	2×10^{-10}
9-m Corner Drop (Initial Impact)	84	8×10^{-6}	2×10^{-6}	8×10^{-10}
9-m End Drop (Slap down)	2	3×10^{-7}	2×10^{-7}	1×10^{-5}
9-m Side Drop	0	5×10^{-7}	7×10^{-7}	2×10^{-5}
0.3-m Side Drop	0	4×10^{-8}	1×10^{-9}	1×10^{-8}
15 × 15 PWR				
9-m End Drop	90	7×10^{-6}	8×10^{-7}	6×10^{-10}
9-m Corner Drop (Initial Impact)	84	9×10^{-6}	1×10^{-6}	2×10^{-9}
9-m End Drop (Slap down)	2	2×10^{-4}	2×10^{-5}	2×10^{-5}
9-m Side Drop	0	2×10^{-4}	5×10^{-5}	2×10^{-5}
0.3-m Side Drop	0	3×10^{-7}	2×10^{-8}	3×10^{-8}

*Sanders, T.L., K.D. Seager, Y.R. Rashid, P.R. Barrett, A.P. Malinauskas, R.E. Einziger, H. Jordan, T.A. Duffey, S.H. Sutherland, and P.C. Reardon. "A Method for Determining the Spent-Fuel Contribution to Transportation Cask Containment Requirements." SAND90–2406. Albuquerque, New Mexico: Sandia National Laboratories. November 1992.

Barrett, et al. (1993) reported single fuel rod failure probabilities in a 9-m [30-ft] drop accident of transportation casks for Westinghouse 17 × 17 PWR SNF with burnup less than about 50 GWd/MTU and General Electric 7 × 7 BWR SNF with burnup less than about 40 GWd/MTU. They reported the probability of forming a longitudinal slit at two different temperatures—27 °C [80 °F] and 149 °C [300 °F]. The estimated probability values, given in Table 3-3, show that the temperature of the cladding has a significant influence on the probability of a slit formation in a fuel rod due to a drop event. However, Barrett, et al. (1993) did not discuss the methodology used to estimate these probabilities. Details of the analysis including the failure used (for either a tear or a slit formation) are not given. Consequently, absence of this important information did not allow critical assessment of the reported results. Therefore, these probability values are not included in Table 2-2.

High-Burnup Fuel

EPRI (2006a) used the Zircaloy cladding material model (EPRI, 2004) to estimate the Mode I/Mode II failure sequence in a 9-m [30-ft] drop of a transportation cask. In high-burnup fuel under long-term dry storage, zircaloy cladding will have both radially and circumferentially oriented hydride platelets distributed nonuniformly through the cladding thickness (EPRI, 2004). Due to this nonuniform distribution of hydrides, the cladding will develop locally varying properties, which can significantly influence the cladding behavior under impact loads. This cladding is modeled as three-phase material with a metal matrix embedded with circumferential and radial hydrides as lamellar structures (EPRI, 2004). Strain normal to the radial hydrides progressively reduces the stress-carrying capacity in both hydrides and matrix. Similarly, strain normal to the circumferential hydrides also causes gradual loss of stress-carrying capacity in both hydrides and matrix; however, the magnitude of this contribution is dependent on the volume fraction of radial hydrides (EPRI, 2004).

Based on the results of the analysis, EPRI (2006a) reported that at the instant of Mode I failure initiation, the peak axial force and the bending moment were approximately 5.3 kN [1,124 lb] and 0.15 m-kN [150 in-lb]. Only 5 percent of the fuel rods experienced axial forces larger than 5.34 kN [1,200 lb]. EPRI (2006a) concluded that guillotine break of the fuel rods does not occur; only partial Mode II tearing can happen, which is predicted to extend over 75 percent of the cross-section. EPRI (2006a) estimated not more than 2.5 percent of the fuel rods, or seven rods in each assembly in a 24-assembly transportation cask, would experience the partial Mode II tear with a similar fraction experiencing smaller transverse tearing.

Table 3-3. Estimated Failure Probability in Different Drop Scenarios Analyzed by Barrett, et al. *

Assembly Type	Drop Orientation	Probability of Single Rod Failure		
		Tear	Slit at 27 °C [80 °F]	Slit at 149 °C [300 °F]
General Electric 7 × 7 BWR	End	2.7×10^{-7}	2.2×10^{-3}	8.3×10^{-7}
General Electric 7 × 7 BWR	Side	2.0×10^{-7}	2.4×10^{-3}	6.3×10^{-7}
Westinghouse 17 × 17 PWR	End	1.1×10^{-4}	2.6×10^{-4}	2.7×10^{-8}
Westinghouse 17 × 17 PWR	Side	3.3×10^{-3}	3.1×10^{-4}	6.8×10^{-8}

*Barrett, P.R., H. Foadian, Y.R. Rashid, K.D. Seager, and S.E. Gianoulakis. "Spent Fuel Assembly Source Term Sensitivity Parameters." High Level Radioactive Waste Management: Proceedings of the 14th Annual International Conference, Las Vegas, Nevada, April 26–30, 1993. La Grange Park, Illinois: American Nuclear Society and American Society of Civil Engineers. pp. 886–892. 1993.

EPRI (2006b) showed that a very small amount of pinch force would be necessary to close the gap between fuel and cladding. Therefore, the possibility that a through-wall fracture would grow without experiencing pellet resistance is small. EPRI (2006b) used the concept of strain energy density (SED) as the demand parameter and the critical strain energy density (CSED) as the capacity parameter to estimate the probability of Mode III failure. Unlike Sanders, et al. (1992), who assumed PCI cracks would grow and develop into longitudinal (Mode III) cracks; EPRI assumed that damage in radial hydrides would initiate a Mode III crack. The probability distributions of SED and CSED are dependent on many factors, such as pinch force, fuel-cladding gap dimension, circumferential and radial hydride concentrations, and cladding temperature. Additionally, each of these parameters is represented by its own distribution. EPRI (2006b) estimated the probability of longitudinal crack formation using Monte Carlo simulation of the SED and CSED. Using 100,000 samples, EPRI (2006b) estimated 2.47 percent of the fuel rods would have some kind of Mode III failure initiated at the cladding internal diameter. Complete through-wall failure of a rod was estimated to be 2×10^{-5} per rod. Therefore, approximately 0.005 rods in each assembly would be expected to have a through-wall longitudinal slit of the cladding in a 9-m [30-ft] accidental drop event during transportation. EPRI (2006b) concluded that the through-wall failure would be pinhole type, which has limited release consequences.

3.1.2 Parameter $n_{tears/rod}$

NUREG–1864 (NRC, 2007, Appendix D) assumed for high-burnup BWR SNF that five breaches would form along a failed rod of high burnup BWR {45–62.5 GWd/MTU for a 30.5 m [100 ft] drop}. Additional information was not given to support the selection of this value for this parameter. This value has been given in Table 2-1. No information is available in the literature for the number of breaches per failed rod for low-burnup PWR and BWR fuel and for high-burnup PWR fuel for a 9-m [30-ft] drop.

3.1.3 Parameters l_c and w_c

NUREG–1864 (NRC, 2007, Appendix D) acknowledged that no information is available on the distribution of the size of cladding fractures due to a drop of a transportation cask. NUREG–1864 assumed that these fractures would be half-circumferential cracks with an aspect ratio of 10. For high-burnup BWR SNF rods, NUREG–1864 assumed that fractures formed in a hypothetical 9-m [30-ft] drop event would have a length of 17 mm [0.7 in] and a width of 1.7 mm [0.07 in].

No information is available on the length or width of fractures formed due to a hypothetical 9-m [30-ft] drop of low-burnup fuel rods as stated in Table 2-2. EPRI (2006a) concluded that full guillotine break of a fuel rod inside a transportation cask would not occur in a 9-m [30-ft] drop and estimated that partial Mode II tearing of 75 percent of the cross-section would occur for high-burnup PWR fuel rods. EPRI (2006a) estimated that the partial Mode II tears would have an opening of 2 mm [0.08 in] at the widest point for a tear decreasing to zero at the root of the tear. However, the failure criterion used by EPRI may not be unique as discussed in Section 3.2 where a knowledge gap is identified.

3.2 Knowledge Gaps on Fuel Rod Response

Cladding fracture toughness and ductility data for higher burnup SNF are sparse. It is reasonable to assume that the outer hydride rim of the cladding will have relatively lower

fracture toughness compared to the inner part of the wall; however, no measurements are available to confirm this. Obtaining additional data on cladding ductility as a function of hydride reorientation is considered to be a high priority (Einziger and Beyer, 2007). Additionally, EPRI has assessed the failure of the Zircaloy cladding under impact load from a drop of the transportation cask by computing the SED ($\mathrm{SED} = \int \sigma_{ij}\, d\varepsilon_{ij}$), where σ is stress and ε is strain, and i, j = 1, 2, 3, and comparing the calculated value with the critical SED. CSED is considered a measure of the failure potential of the cladding. The strain energy density concept has been used by others to predict fracturing of brittle materials (e.g., Mecham, et al., 1983). Mecham, et al. (1983) used this SED parameter to correlate with total fracture surface area of glass, ceramic, and quartz and ultimately with the fragment size distribution using a log-normal particle size distribution. Rather than a unique parameter, SED is a product of two parameters. Although both stress and strain can be instrumental to fuel rod response, additional supporting data are needed to corroborate the appropriateness of using the SED–CSED concept to estimate cladding failure (in Mode I leading to Mode II, which uses K_{IC} concept, and Mode III).

It seems that CSED may not be a unique parameter describing the capacity (strength) of fuel cladding. CSED may differ for the same material depending on the loading conditions (or failure mechanism involved) (e.g., tensile versus impact versus creep). Consequently, a set of CSED values would be needed for a range of stresses (and temperatures) to address each application; however, CSED is generally estimated from tensile test data. It is also not clear whether SED explicitly incorporates information on the size of the inherent crack (or flaw) population. It may so happen that the size of the most critical flaw in the material would control the survivability of the cladding. It is also not clear how loading rate dependent strength is incorporated in CSED determination. Therefore, a knowledge gap exists for predicting the failure of high-burnup fuel cladding under impact load. High priority should be given to addressing this lack of a suitable failure criterion to predict cladding failure under impact loading.[1]

[1]NRC does not accept the CSED methodology to determine cladding failure due to vast scatter in the baseline data.

4 FUEL PELLET RESPONSE ASSESSMENT

This chapter discusses current knowledge of fuel pellet responses due to impacts. Recommended values were derived from available literature for fuel response parameters related to release fraction estimates. Knowledge gaps pertaining to fuel pellet responses to impacts and release fraction estimates are also discussed.

4.1 Existing Knowledge and Selection of Values for Fuel Pellet Response

Factors important to fuel fracturing and releases of radioactive material into the canister are the fuel type, characteristics of the rim and its response to impacts, characteristics of fuel body and its response to impacts, fuel rod thermal history, radionuclide inventory, and distribution. When the cross-section average burnup exceeds approximately 45 GWd/MTU, the microstructure of the pellet periphery is markedly changed (Matzke and Spino, 1997), and the term "rim" is used to differentiate the pellet periphery from the internal fuel pellet (or body). Available information on fuel pellet response was assessed in the context of individual parameters (refer to Figure 2-1). Radionuclide inventory and its distribution within the fuel pellet, including the concentration of certain radionuclides in the rim region for high-burnup fuel have been addressed by others [Noirot, et al., 2008; Dehaudt, 2001; Lozano, et al., 1998; Koo, et al., 2001; Rondinella and Wiss, 2010; Sprung, et al., 2000; NRC, 2007, Appendix D, Eqs. (D.2) and (D.6)]. Recommended values for fuel pellet parameters are presented in Tables 2-1 and 2-2.

4.1.1 Parameter $F_{init,body}$

Respirable fuel particles (i.e., aerodynamic diameter less than 10 μm) can be generated by mechanical damage, such as abrasion during insertion of the fuel pellet into the rod and cracking of the fuel pellets during reactor operation, even without impact loading from a drop event. NUREG–1864 (NRC, 2007) used the results of burst tests of low-burnup PWR fuel (up to 31 GWd/MTU) rod segments at temperatures of 900 to 1,100 °C [1,652 to 2,012 °F] conducted by Lorenz, et al. (1980). Lorenz, et al. (1980) measured the size and mass fraction of the fuel particulates that escaped from the burst sites. Measurements indicate that the mass fraction of respirable fines is approximately 4×10^{-6}. Considering the size of burst openings and the 99 percent filtering efficiency, NUREG–1864 (NRC, 2007, p. D–10) assigned a value of 2.4×10^{-5} (Table 2-2) for the $F_{init,body}$ parameter for the respirable particulates from low-burnup (both PWR and BWR) fuels. NUREG–1864 (NRC, 2007) did not assign a value for the $F_{init,body}$ parameter for high-burnup BWR fuel because no information from similar tests for high-burnup BWR fuel was available when the document was published.

Hanson, et al. (2008) conducted pressurized flow tests for high-burnup fuel rod segments and measured the size of released fuel particles. The release of fuel particulates from the breached rods was accomplished by flowing a continuous stream of dry air through the porous internal structure of the fuel segments within cladding. For the case of PWR fuel with a burnup of 45 GWd/MTU, the fractional release, calculated using an optical particle counter, ranged from 1×10^{-5} to 8×10^{-5}. The release from BWR fuels with a burnup of 53–69 GWd/MTU ranged from 9×10^{-7} to 1.6×10^{-5}. Considering the similarity of material characteristics of the fuel body between and the low and high-burnup fuels (i.e., similar grain size and porosity), the range of the fractional release of the high-burnup PWR and BWR fuels reported in Hanson, et al. (2008) appears reasonable. Therefore, the ranges for the $F_{init,body}$ parameter are assigned to be

9×10^{-7} to 1.6×10^{-5} for high-burnup BWR SNF (Table 2-1) and 1×10^{-5} to 8×10^{-5} for high-burnup PWR SNF (Table 2-2).

4.1.2 Parameter $F_{init,rim}$

The rim region, in contrast to the fuel body, will not sustain abrasion damage during reactor operation. Consequently, Einziger (2007) argued that the parameter ($F_{init,rim}$) for the initial respirable fraction from the rim region should be zero. No new information was found in the literature for the $F_{init,rim}$ parameter (Table 2-2).

4.1.3 Parameter $F_{imp,body}$

Jardine, et al. (1982) conducted impact tests of various brittle materials including glass, ceramic, and unirradiated UO_2 pellets and measured the size of the resulting fractured fuel particulates. For UO_2 pellets, the measurement results indicate approximately 0.02 percent of the respirable fraction at the impact energy density of 1.2 J/cm^3, gives 2×10^{-4} of the respirable fraction. Based on the results performed by Jardine, et al. (1982), the equation to obtain F_{imp} of brittle materials is formulated as a function of impact energy (DOE, 1994)

$$F_{imp} = A(\rho gh) = A\left(\frac{E}{V}\right) = A\left(\frac{\rho E}{m}\right) \quad (4\text{-}1)$$

where A is the empirical correlation (2×10^{-11} cm^3/erg or 2×10^{-4} cm^3/J); *g* is the acceleration due to gravity; *h* is the height of drops; E is the impact energy ; and V, m , and ρ are the volume, mass, and density of brittle materials, respectively.

In NUREG–1864 (NRC, 2007), the mass fraction of respirable fuel particulates of the irradiated UO_2 fuel (up to average burnup of 33 GWd/MTU) is assessed using Eq. (4-1). The comparison reveals that the mass fraction of the irradiated UO_2 fuel is smaller than the values present in the DOE handbook by an order of magnitude irrespective of the impact energy. Thus, to be applicable to low-burnup and high-burnup fuels, the value of A presented with Eq. (4-1) was reduced by a factor of 5 in NUREG–1864 (NRC, 2007). Using Eq. (4-1) with the reduced A value, a UO_2 pellet density of 10.96 g/cm^3, and the acceleration due to gravity of 9.8 m/s^2 for a 9-m [30-ft] drop impact, the $F_{imp,body}$ parameter is 4×10^{-5}. This result is identical to the value reported in Einziger (2007). No new information was found in the literature for the $F_{imp,body}$ parameter.

4.1.4 Parameter $F_{imp,rim}$

The $F_{imp,rim}$ parameter is defined as the fraction of mass of UO_2 in the rim layer of a SNF pellet that is converted to respirable fuel fines by brittle fracture due to the impact. NUREG–1864 (NRC, 2007, p. D–11) acknowledged that an uncertainty of several orders of magnitude exists in estimates for $F_{imp,rim}$. A range was assumed for $F_{imp,rim}$ in which the $F_{imp,body}$ parameter value was adopted as the low value. Complete fracture was assumed for the high value of the range.

The release fraction of fuel particulates from the rim due to an impact depends on the microstructure and mechanical properties of the rim region. Features of the rim microstructures and results of mechanical tests conducted in the rim region are discussed below. Finally, the recommended value of the parameter $F_{imp,rim}$ is discussed.

Considerations for High-Burnup Spent Fuel

Currently, most of the discharged SNF from a reactor has a burnup in excess of 45 GWd/MTU (McKinnon and Cunningham, 2003). The operating burnup limit of the reactors is currently restricted to 62.5 GWd/MTU (peak rod) (Brach, 2003). When the cross-section average burnup exceeds approximately 45 GWd/MTU, as commonly observed, the microstructure of the pellet periphery or rim is markedly changed (Matzke and Spino, 1997), due to locally high burnup. The local burnup in the rim is approximately 1.3 times higher than the average pellet burnup (Koo, et al., 2001). This rim structure is generally characterized by several unique features, such as (i) submicron sized grains (0.1 to 0.3 μm), (ii) high porosity (up to more than 25 percent) with many faceted micro size pores, (iii) high concentrations of actinides (approximately 2 times higher Pu and Np concentrations compared to the fuel body) and high fission gas retention in pores, and (iv) Xe depletion (Spino, et al., 2003; Matzke and Spino, 1997; Noirot, et al., 2008; Lozano, et al., 1998; Koo, et al., 2001; Rondinella and Wiss, 2010). Because the characteristics of the rim structure (submicron size grains and high porosity) and chemistry (high actinide concentration) will affect the fuel fracture responses to impact and, therefore, the source term, the potential contribution of the rim structure to the respirable fraction needs to be evaluated.

Rim Thickness and Its Volume Fraction

Due to relatively high concentrations of actinides and fission gas retained in the rim, knowing the rim thickness is important for determining the radionuclide inventory and its potential effect on source term when high-burnup fuel rods are breached in an impact. The rim thickness generally increases with fuel burnup. Using measurement results of grain size and porosity obtained by optical microscopy and Xe concentrations determined by electron-probe microanalysis, a correlation of rim thickness with burnup was measured by several researchers.

Einziger and Beyer (2007) observed that the rim thickness, t, increases with burnup according to the following relationship

$$t\ (\mu m) = 1.439 \times 10^{-6} \times \text{AVE BU}^{4.43} \qquad (4\text{-}2)$$

where, AVE BU is the average pellet burnup (GWd/MTU).

Koo, et al. (2001) developed linear equations for the rim thickness as a function of the rim average burnup by fitting the measured data on rim thickness using a linear least-square method. The mean rim thickness is estimated by

$$t\ (\mu m) = 3.55 \times \text{RIM BU} - 185 \qquad (4\text{-}3)$$

where, RIM BU is the average rim burnup (GWd/MTU).

Koo, et al. (2001) also developed the following equation to represent the upper bound of the rim thickness

$$t\ (\mu m) = 5.28 \times \text{RIM BU} - 178 \qquad (4\text{-}4)$$

Note that Koo, et al. (2001) used the average rim burnup and not the average pellet burnup in estimating the rim thickness.

Using these three equations [Eq. (4-2), (4-3), and (4-4)], the rim thickness is calculated as a function of the average pellet burnup and the results are presented in Figure 4-1. To compare the calculated rim thickness using equations with a linear and an exponential increase, the average rim burnup is converted to the average pellet burnup by dividing the average rim burnup by a factor of 1.3 (Koo, et al., 2001). For example, the average pellet burnup of 60 GWd/MTU can represent an average rim burnup of 78 GWd/MTU.

As seen in Figure 4-1, for 60 GWd/MTU, the thickness can vary from approximately 100 μm using Eq. (4-3) to 230 μm using Eq. (4-4). Note that these three equations [Eq. (4-2), (4-3), and (4-4)] do not explain the possible difference of rim thickness between PWR and BWR high-burnup fuels. Assuming a fuel pellet with length of 1 cm [0.394 in] and radius of 0.5 cm [0.197 in], the calculated volume fraction of the rim layer is shown in Figure 4-2. The volume fraction of the rim layer is obtained by subtracting the volume of the fuel body from the total volume of 0.786 cm^3 for a pellet.

As seen in Figure 4-2, at 60 GWd/MTU, the volume fraction of the rim varies from 3.6 to 9.1 percent, which yields an average volume fraction of 6.4 percent. By applying a factor of two for the actinide concentration in the rim compared to the fuel body for the high-burnup fuel (Dehaudt, 2001), the mass fraction of radionuclide inventory in the rim region, specifically for actinides (Pu and Np), can range from 7.2 to 18.2 percent. Accordingly, the mass fraction of actinide in the fuel body can range from 92.8 to 81.8 percent. Therefore, average fractions of actinides would be 13 and 87 percent in the rim and the fuel body, respectively. The average fraction of 13 percent in the rim calculated in this study is slightly higher than the fractions of 11.3 percent for the rim as adopted in NUREG–1864 (NRC, 2007). Because the fractions in NUREG–1864 (NRC, 2007, Section D.2.4) were based on a typical BWR rod and may have used different dimensions for the pellet, the mass fractions obtained in this study could be different depending on the pellet dimension, fuel burnup level, and total inventory.

Rim Hardness and Fracture Toughness

Spino, et al. (2003) measured the mechanical hardness of the irradiated UO_2 fuel (burnup between 40 to 80 GWd/MTU) by conducting Vickers hardness indentation tests with relatively low indentation loads up to 1 N [0.2 lb]. The results revealed that the hardness measured for the rim region was lower than the central part of fuel body by up to 30 percent. The hardness gradually decreased toward the pellet edge (so called “softening” in the rim) and this decrease was correlated with high porosity in the rim. The crack length propagated from the indented area was up to 6 μm at the pellet edge and 9 μm in the fuel body. Matzke and Spino (1997) estimated the fracture toughness of the rim by combining the other parameters (i.e., Young’s modulus and imprint half-diagonal length) with the measured crack length. The fracture toughness, K_{IC} was estimated to be up to ~2.7 MPa $m^{½}$ at the pellet edge and ~1.3 MPa $m^{½}$ in the fuel body (about 2 times higher fracture toughness in the rim region compared to the fuel pellet body). The K_{IC} of the fuel pellet body was comparable to the unirradiated UO_2 matrix. The authors explained that the increased fracture toughness in the rim region was mainly due to high porosity in the rim based on the observation of short crack length in the rim and local crack blunting (deflection) at the pore front and bridging (branching). In the micrograph of the fractured rim area, crack propagation appeared to proceed through grain boundaries (i.e., intergranular cracking), while fuel pellet body fracturing was caused by transgranular cracking.

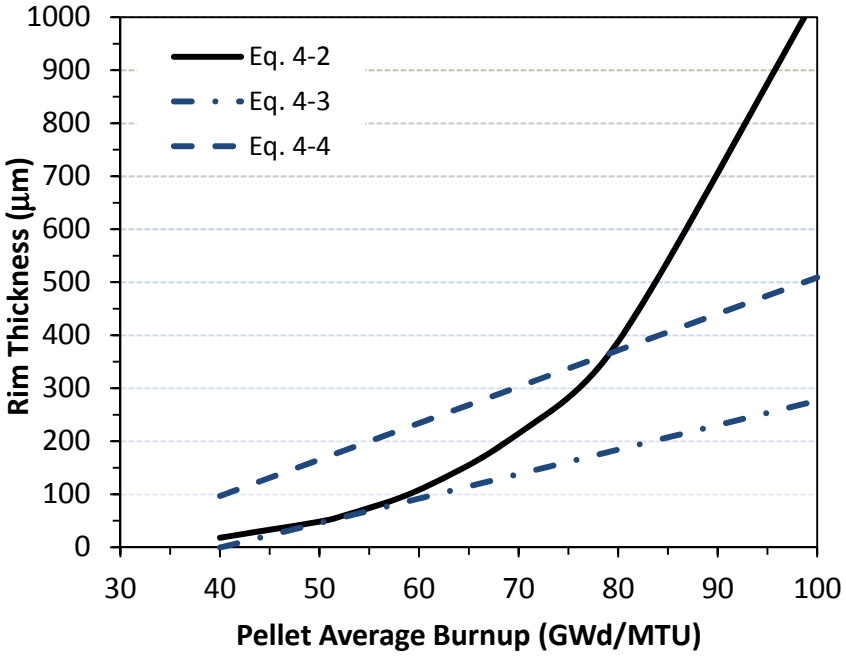

Figure 4-1. Rim Thickness (µm) As a Function of Pellet Average Burnup

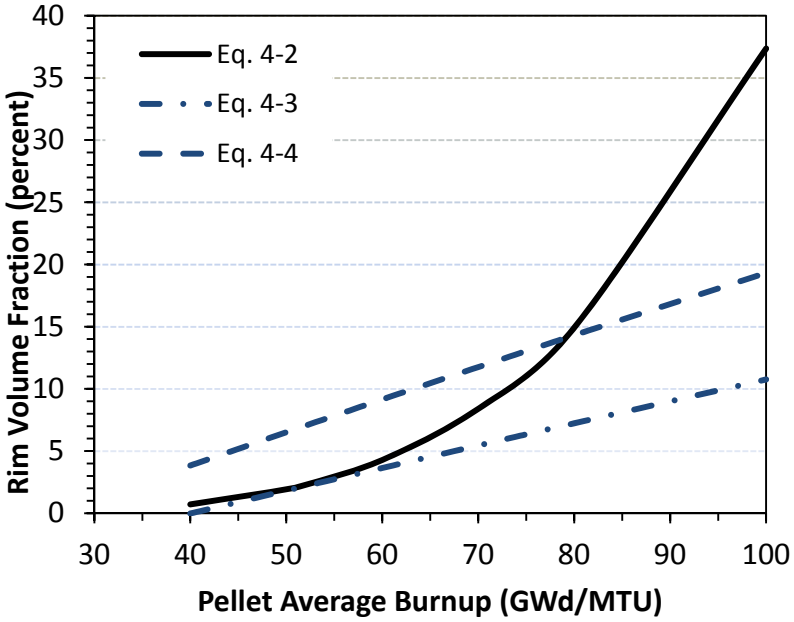

Figure 4-2. Rim Volume Fraction (Percent) As a Function of Pellet Average Burnup Assuming a Pellet Length of 1 cm [0.39 in] and Radius of 0.5 cm [0.2 in]

Similar observations for sintered UO_2 were reported by Kapoor, et al. (2007) based on Vickers indentation test results measured with a relatively high load of 10 N [2.2 lb]. The estimated fracture toughness in the fine-grained area (~10 μm grain size) with high porosity was higher than the relatively coarse-grained area (appeared ~30 μm grain size) with relatively low porosity by a factor of 10 to 20. Even the estimated fracture toughness [K_{IC} of 2–5 MPa $(m)^{½}$] was relatively high for the small-grained area with high porosity. The crack length in the small-grained area reached 30–40 μm and cracks propagated either by intergranular cracking at the grain boundary channel-type porosity or by transgranular cracking at the large rounded porosity area. Similar to Matzke and Spino (1997), cracks propagated by transgranular cracking in the coarse-grained area containing fine intragranular porosity.

The increase of fracture toughness of the porous rim region (Matzke and Spino, 1997) and the small porous-grained area (Kapoor, et al., 2007) appears somewhat contrary to the commonly observed behavior for typical brittle materials; the mechanical strength and fracture toughness decreases with porosity in coarse-grained UO_2 (Wagh, et al., 1993) and other ceramics such as Si_3N_4, alumina, and $YBa_2Cu_3O_7$ (Rice, et al., 1985; Singh, et al., 1989). With increasing porosity, both hardness and fracture toughness usually decrease, making the material more fragile to impact. Winnubst, et al. (1983) conducted bend tests of single-phase yttria-stabilized zirconia ceramics having a grain size of 0.6 to 50 μm. The results revealed that high porosity led to a decrease in the Young's modulus and toughness. The fracture toughness tends to decease with porosity. Grain size refinement appeared to play a minor role in the fracture toughness. By comparing the values for fracture toughness of the same materials obtained by Vickers indentation measurement, Winnubst, et al. (1983) found the bend test technique to be more consistent in estimating fracture toughness because the crack dimensions using the indentation technique can be affected by grain size, surface roughness, surface stress, and the level of load.

While the porosity present in brittle materials tends to reduce the mechanical properties such as Young's modulus and fracture toughness, grain size refinement in crystalline materials increases the mechanical strength according to the well known Hall-Petch strengthening mechanism (the yield strength of dense crystalline materials increases as grain size deceases). When only considering the submicron size grains in the rim, one can expect a relatively high yield strength in the rim compared to the coarse grain-sized fuel pellet body. However, the rim also contains relatively high concentrations of micron-sized pores that can lead to a decrease in the mechanical strength and likely to a decrease in the fracture toughness. Because fracture toughness should be more closely correlated with the specific surface energy of the fracture surface, it is not always true that high strength will result in high fracture toughness. For the case of fine-grained ceramics, it is reported that the fracture toughness increased slightly or remained constant with decreasing grain size (Zimmermann, et al., 1998). Therefore, two opposite effects occur; grain refinement increases the mechanical strength whereas high porosity tends to decrease the mechanical strength and fracture toughness in the rim structure. The occurrence of these two competing effects makes it difficult to determine their contributions to fracture toughness.

Potential Rim Responses to Impact

As discussed in the previous section, there was an observation that intergranular cracking tends to occur in the relatively small grained area with high porosity and the rim region. This indicates that the rim region can create more respirable particles when the impact energy is high enough to produce grain sized fracturing. In EPRI (2005b), for the case of a 9-m [30-ft] drop event, the

stress intensity factor (K_{IC}) induced on the fuel rod by impact was estimated to be higher than 16 MPa $m^{1/2}$. Obviously, the value of 16 MPa $m^{1/2}$ is higher than the K_{IC} values of the high-burnup fuel pellet [i.e., 1.3 to 2.7 MPa $m^{1/2}$ by Matzke and Spino (1997)]. Thus, if this high level of stress is transferred to the fuel pellet, the rim may fracture extensively and produce more respirable fuel particles. Contact of the clad rod with the fuel pellet by swelling, specifically for the high-burnup fuel, can transfer stresses induced on the rod surface to the pellet.

The high-pressure of the rim bubbles as presented in Lozano, et al., (1998) and Koo, et al. (2001) can also break apart the rim region at the grain boundaries by lowering the impact energy required to fracture the grain boundaries. The results of recent reactivity initiated accident tests of high-burnup fuel demonstrated that the fuel was fragmented and fractured into less than 10 μm size due to high thermal energy during the reactivity initiated accident test (Une, et al., 2006). In scanning electron micrographs of the fractured particles, subdivided grains with submicron sizes and many rim bubbles were also evident.

There are currently no reported data on rim fracture formation as a function of impact energy in the literature. Given the uncertainties in estimating the respirable fraction in the rim without experimental data, the $F_{imp,rim}$ and its related source term should have a relatively large variation such as several orders of magnitude. NUREG–1864 (NRC, 2007, Section D.2.4.1.2) and Einziger (2007) suggest that the values of $F_{imp,rim}$ can range from 4×10^{-5} to 1, where 4×10^{-5} represents the rim having the same fracture behavior as the fuel body and 1 represents complete fracturing of the rim layer into particulates with diameters less than 10 μm. As presented in NRC (2007, Appendix D), the particle release fraction, $F_{RC,k}$ can vary three orders of magnitude due mainly to large variation of $F_{imp,rim}$.

4.1.5 Parameter R_{RCg}

Parameter R_{RCg} is the fraction of fission gas released from the rod after fracture. The release fraction of fission gas from a fuel rod in a hypothetical drop event was presented in NUREG–1864 (NRC, 2007, p. D–15) to range between 0.12 (12 percent) and 0.4 (40 percent).

Compared to micro structural changes in the rim of a fuel pellet for burnup exceeding 45 GWd/MTU, the linear power rating of fuel has a greater effect on fission gas release (FGR). Because a high linear power rating at moderate burnup can lead to very high FGR, this factor should be considered in assessing fission product release. Johnson, et al. (2012) presented measured FGR data for high-burnup PWR fuels and a high-burnup BWR fuel (Table 4-1). The data illustrate that the higher FGR is observed at high linear power ratings. This is likely the explanation for the high (20.6 percent) measured FGR for the Gösgen PWR fuel. It can be seen from the data that for PWR fuel, the total potential FGR from the gap release and fission gas present in rim pores could be as high as 20.6 percent at a burnup of 64 GWd/MTU.

Johnson, et al. (2012) also presented data for the segregation of fission gas from the fuel grains into pores within the rim for a typical PWR fuel. This was estimated based on a model by Koo, et al. (2001), and is given in Table 4-2.

In a hypothetical drop event, the fission gas in the rim region could potentially be released if the rim fractures along the grain boundaries. Using the pessimistic estimate from Table 4-2, this could result in release (gap + rim pores) of up to 4 percent for PWR fuels with burnup less than 45 GWd/MTU) and up to 20.5 percent for PWR fuels with burnup of 60 to 75 GWd/MTU.

Table 4-1. Fuel Irradiation History and Measured Fission Gas Release*						
Reactor	Type	Burnup (GWd/MTU)	No. Cycles	Peak Linear Power Rating at 40 GWd/MTU	Measured FGR%	Error
Leibstadt (BWR)	UO_2	65.3	7	23	3.69	± 0.1
Gösgen (PWR)	UO_2	64	4	28.5	20.6	± 0.5
Ringhals (PWR)	UO_2	58.2	5	20	0.94	± 0.1
Ringhals (PWR	UO_2	61.4	5	23	2.3	± 0.2
Ringhals (PWR)	UO_2	66.5	5	22	2.6	± 0.2
North Anna (PWR)	UO_2	75.4	4	23	5	± 0.3

FGR = Fission Gas Release

*Johnson, L., I. Günther-Leopold, J. Kobler Waldis, H.P. Linder, J. Low, D. Cui, E. Ekeroth, K. Spahiu, and L.Z. Evins. "Rapid Aqueous Release of Fission Products From High Burn-Up LWR Fuel: Experimental Results and Correlations With Fission Gas Release." *Journal of Nuclear Materials.* Vol. 420. pp. 54–62. 2012.

Table 4-2. Fission Gas Release and Fraction of the Total Fission Gas Inventory in a Fuel Rod in the Rim Pores of Pressurized Water Reactor UO_2 Fuel (Johnson, et al.);* Best Estimate Values; Pessimistic Estimate Values Based on a Model by Koo, et al.†				
Average Burnup (GWd/MTU)	Rim Burnup (GWd/MTU)	Typical FGR%	Percent of Total FG Present in the Rim Pores in BE	Percent of Total FG Present in the Rim Pores in PE
37	49	0.3	0	0
41	55	0.4	0	0.5
48	64	1.0	2	3
60	80	3.6	4	8
75	100	6.5	8	14

FGR = Fission Gas Release
FG = Fission Gas
BE = Best Estimate
PE = Pessimistic Estimate

*Johnson, L., I. Günther-Leopold, J. Kobler Waldis, H.P. Linder, J. Low, D. Cui, E. Ekeroth, K. Spahiu, and L.Z. Evins. "Rapid Aqueous Release of Fission Products From High Burn-Up LWR Fuel: Experimental Results and Correlations With Fission Gas Release." *Journal of Nuclear Materials.* Vol. 420. pp. 54–62. 2012.
†Koo, Y.-H., B.-H. Lee, J.-S. Cheon, and D.-S. Sohn. "Pore Pressure and Swelling in the Rim Region of LWR High-Burnup UO_2 Fuel." *Journal of Nuclear Materials*. Vol. 295. pp. 213–220. 2001.

Johnson, et al. (2005) presented measured FGR data from PWR fuels with burnup from 20 to 65 GWd/MTU. The measured FGR (gap region) is nominally below about 1 percent for low-burnup fuels. However, above 50 GWd/MTU, the FGR (gap) increases to a value of about 6 percent or less.

Koo, et al. (2001) derived a relationship between rim burnup and pellet-average burnup based on measured data relevant to typical light water reactor operation. Koo, et al. (2001, Figure 4) presented the fractional Xe in rim pores as a function of rim burnup. This figure shows that for rim burnup from 60 to 80 GWd/MTU (equivalent to pellet-average burnup from 45 to 60 GWd/MTU) the fractional Xe in rim pores ranges from ~5 to 12 percent. For rim burnup less than 60 GWd/MTU with little to no rim formation (about 45 GWd/MTU), the fractional Xe in rim pores is <5 percent. Using an assumption that no gas is released from the rim and all Xe atoms depleted from the rim matrix are retained in the rim pores, the maximum depleted fraction of 20 percent was obtained for the pellet with average burnup of 80 GWd/MTU, which is comparable to measured values in the literature examined by Koo, et al. (2001).

The Nuclear Energy Agency (2010) reviewed reactivity-initiated accident effects on fuel and cladding behavior. In these tests, short fuel test rods, generally fabricated from pre-irradiated full-length rods, were subjected to power pulse transients in various test reactors. The transients cause rapid pulses in fuel temperature, which induce stresses in the fuel rods and in most cases results in fuel cracking and fragmentation (and in some cases, fuel cladding failure).

Grain boundary decohesion results in burst release of fission gases and helium (generated from alpha-decay), stored in intergranular bubbles and pores. Papin, et al. (2007) estimated that the rim structure in high-burnup UO_2 fuels accounts for half of the total grain boundary gas inventory and about 10 percent of the total gas inventory in the pellet. Nuclear Energy Agency (2010, Appendix A) summarized FGR results from reactivity-initiated accident tests on low-burnup and high-burnup PWR and BWR fuels. The FGR data from those fuels that did not fail during the test are summarized in Tables 4-3 and 4-4. The data represent tests reported in the literature up to March 2009. Transient release of retained fission gases typically ranged from 5 to 25 percent of gas produced and accumulated in the rodlets for PWR fuels and from 3 to 17 percent for BWR fuels. Data for PWR fuels with burnup less than 45 GWd/MTU indicate a transient gas release ranging from 3.5 to 20 percent. As fuels with burnup less than approximately 50 GWd/MTU do not form rims, the high FGR is likely from fracture of grain boundaries throughout the fuel. For PWR fuels with burnup greater than 45 GWd/MTU, transient gas releases ranged from 5.9 percent to 26 percent and would represent release from rim grain boundaries and from the interior pellet region. For BWR fuels with burnup less than 45 GWd/MTU, transient gas releases ranged from 4.7 to 15 percent and for burnup greater than 45 GWd/MTU, transient gas releases ranged from 3.1 to 15.7 percent.

Rossiter and Mignanelli (2011) presented a graph of measured FGR data for Fragema PWR and BWR fuels. PWR fuels showed FGR of less than 1 percent for low-burnup (<45 GWd/MTU) and increasing releases from 1 to 2.8 percent for burnup from 45 to 60 GWd/MTU. For BWR 8 × 8 fuels, there was a large scatter in measured FGR, ranging from 5 to approximately 28 percent for burnup from 25 to 45 GWd/MTU with no clear dependence on burnup. The scatter for 8 × 8 fuels was attributed to higher linear power ratings for the same assembly power and larger pellet diameters giving higher fuel centerline temperatures for a given local power rating. The data for 8 × 8 fuel assemblies may not be relevant to domestic BWR fuels, which have a majority of 9 × 9 or greater fuel rod assembly configurations. For 10 × 10 BWR fuels, the releases were similar to PWR fuels. For burnup less than 45 GWd/MTU, releases were <~2.5 percent and for burnup up to 50 GWd/MTU, FGR ranged from <1 to 5 percent for 10 × 10 BWR fuels.

Hirano, et al. (2005) presented FGR data from BWR fuels. The FGR data for 9 × 9 rods showed releases that were generally independent of burnup. Fission gas release ranged from <1 to <5 percent at burnup from 25 to 60 GWd/MTU. Barrett, et al. (1993) presented FGR data for low-burnup PWR and BWR fuels (i.e., rod-averaged burnup less than 40 and about 50 GWd/MTU, respectively); they suggested upper limits for FGR of 16 and 25 percent, respectively, but noted a large scatter in the data and dependency on power profiles of the fuel rods. Since the Barrett, et al. (1993) study, recent efforts by others [e.g., McKinnon and Cunningham (2003)] have established a more definitive relationship between FGR and burnup.

Table 4-3. Transient Fission Gas Release From Pressurized Water Reactor Pre-irradiated Fuel Rods (Nuclear Energy Agency, 2010)*		
Test ID†	**Burnup (GWd/MTU)**	**Transient FGR (%)**
Nuclear Safety Research Reactor‡		
TK–1	38	20.0
TK–6	38	16.2
MH–1	39	3.5
MH–3	39	4.0
GK–1	42	12.8
TK–5	48	11.1
HBO–7	49	8.5
HBO–2	50	17.7
HBO–3	50	22.7
HBO–4	50	21.1
TK–3	50	10.9
TK–4	50	8.3
TK–8	50	5.9
TK–9	50	6.2
OI–12	61	22.4
RH–1	67	21.4
RH–2	67	26
CABRI§		
REP–Na2	33	5.5
REP–Na3	54	13.7
REP–Na4	62	8.3
REP–Na5	62	15.1
REP–Na11	60	6.8
CIPO–2	75	15.0

FGR = Fission Gas Release

*Nuclear Energy Agency. "Nuclear Fuel Behaviour Under Reactivity-initiated Accident (RIA) Conditions." Appendix A. NEA No. 6847. NEA/CSNI/R(2010)1. Paris, France: Nuclear Energy Agency. 2010.

†Refer to original source (Nuclear Energy Agency, 2010) for test details.

‡Nuclear Safety Research Reactor (NSRR): UO_2 fuel rods were pre-irradiated in pressure water reactors and boiling water reactors in nine different reactors in Japan, Spain, Sweden and USA. Full-length rods were used in the MH and GK series tests and the remainder used ~120-mm [30-in] rodlets fabricated from the full length rods. Fill gas pressures ranged from 0.1 to 5.1 MPa [1 to 50 atm] in order to simulate the range of gas conditions representing end-of-life gas composition and pressure. In the MH and GK series tests, transient fission gas release contributed 4- to 8-MPa [39- to 79-atm] pressure increase in the rods.

§CABRI Reactor: All CABRI test rods had a U-235 enrichment of 4.5 percent except REP–Na2 which was enriched to 6.85 percent. Rod let REP–Na3 was pre-irradiated as a segmented rod while all other rodlets were re-fabricated from full-length PWR fuel rods from commercial reactors. Only data from rodlets that survived the transient test are presented in Table 4-3. The major part of FGR comes from grain boundary gases due to fuel fragmentation, grain boundary opening and fuel permeability evolution. He release up to 30 percent of total fission gas release was measured. Fill gas pressures ranged from 0.3 to 1.5 MPa (3 to 15 atm).

Table 4-4. Transient Fission Gas Release From Boiling Water Reactor Preirradiated Fuel Rods. Parent Fuel Rods Were Preirradiated and Fabricated Into Rodlets for Reactivity Initiated Accident Tests. Fission Gases Were Measured by Puncture Tests.*		
Test ID†	**Burnup (GWd/MTU)**	**Transient FGR (%)**
Boiling Water Reactor Nuclear Safety Research Reactor		
TS–2	26	12
TS–3	26	10
TS–4	26	15
TS–5	26	8
Boiling Water Reactor Nuclear Safety Research Reactor		
FK–3	41	4.7
FK–2	45	8.2
FK–1	45	3.1
FK–4	56	15.7
FK–5	56	9.6
FK–8	61	11.3
FGR=Fission Gas Release *Nuclear Energy Agency. "Nuclear Fuel Behaviour Under Reactivity-initiated Accident (RIA) Conditions." Appendix A. NEA No. 6847. NEA/CSNI/R(2010)1. Paris, France: Nuclear Energy Agency. 2010. †Refer to original source (Nuclear Energy Agency, 2010) for test details.		

McKinnon and Cunningham (2003) illustrated the broad range of in-reactor FGR in the gap observed for PWR-type rods (Figure 4-3). The top of the band is representative of rods held at higher power during irradiation (Manzel and Walker, 2003) and may represent an upper bound FGR. The bottom of the band is representative of rods held at lower power levels (Morel, et al., 1994). Based on Figure 4-3, the FGR from the gap ranges from <1 to 12 percent for burnups less than 45 GWd/MTU and ~2 to ~15 percent for fuels from 45–60 GWd/MTU. Principal observations from a post-storage examination of low-burnup (23–35 GWd/MTU) PWR fuels from a CASTOR–V/21 dry storage demonstration (McKinnon and Cunningham, 2003) indicated that the post-storage gas pressures were 3.4 to 3.6 MPa [34 to 36 atm] {at 300K [80.6 °F]} and FGRs were 0.4 to 1.0 percent.

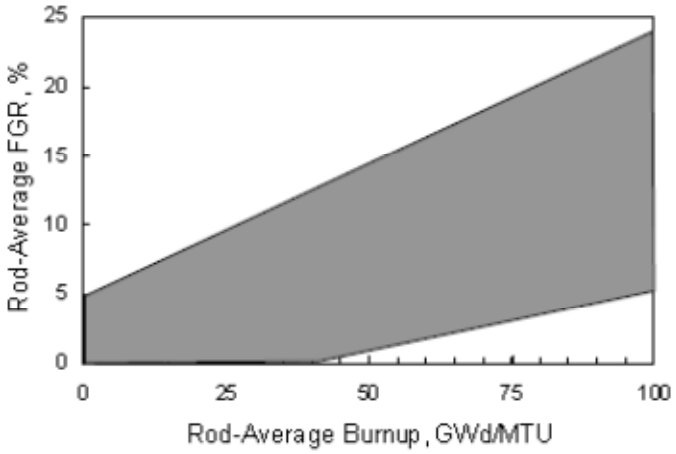

Figure 4-3. Range of Observed Fission Gas Releases to the Gap As a Function of Burnup From Pressurized Water Reactor Fuels (McKinnon and Cunningham, 2003)

Beyer and Clifford (2011) reported on fission product gap inventories and transient gas release based on empirical data for reactivity-initiated accidents. They note that no FGR measurements exist on the potential transient release associated with fragmentation of high-burnup fuel pellets resulting from an assembly drop or fuel rod balloon/burst and that future testing may be necessary to address the potential transient releases resulting from grain boundary separation and fuel fragmentation. The gap release values calculated in their report involve the use of the updated FRAPCON–3.3 fuel performance code (Lanning, et al., 2005) with the 2011 ANS 5.4 standard equations implemented to determine the release-to-birth (R/B) fractions of the volatile radioactive isotopes of noble gases (xenon and krypton), iodine, and cesium. The gap and rim release values proposed are upper bound cases. A bounding power history was used and it was noted that running reactors at the bounding power history would exceed burnup limits in the United States. The derived PWR and BWR Kr-85 bounding gap release fractions based on peak values were 35.7 and 37.2 percent for 14 × 14 and 9 × 9 designs, respectively.

Beyer and Clifford (2011) reviewed stable noble gas release data from simulated reactivity-initiated accident tests on BWR and PWR test rods; these data were also presented in Nuclear Energy Agency (2010). The measured Kr-85 release ranged from 15 to 25 percent for burnup from 45 to above 55 GWd/MTU at peak enthalpy increases above 130 cal/g. It is assumed that significant grain boundary fracturing occurred at these enthalpies. For burnup from 28 to 45 GWd/MTU, releases ranged from 5 to 20 percent. An upper bound Kr-85 release fraction (F) relationship was developed based on the enthalpy increase, ΔH

$$F(^{85}Kr) = 0.0022 * \Delta H \qquad (4\text{-}5)$$

Analysis by Beyer and Clifford (2011) suggests that if significant grain boundary de-cohesion were to occur during a hypothetical drop of a transportation cask, up to ~30 percent of the fission gases retained in grain boundary bubbles could be released. Their analysis of fission gap release suggests an upper bound of 38 percent for both PWR and BWR reactors.

Typical fission gas gap and rim releases are shown in Table 4-5. In addition to Table 4-5, a bounding fission gas gap release of 38 percent was derived by Beyer and Clifford (2011) for both PWR and BWR fuels for burnup and power histories typical of these reactors. The review of reactivity-initiated accident data by Beyer and Clifford (2011) indicated a bounding transient gas release of 30 percent, which is consistent with measured rim releases for high-burnup fuels.

In summary, for low-burnup PWR and BWR fuels, FGR to the gap region is typically less than 1 percent; however, there are isolated cases where releases as high as 15 percent have been observed. Based on isolated observations of higher releases, a value of 5 percent is selected

Table 4-5. Typical Fission Gas Releases From the Gap Fuel Body and Rim

Pressurized Water Reactors		**Boiling Water Reactors**	
<45 GWd/MTU	**45–62.5 GWd/MTU**	**<45 GWd/MTU**	**45–62.5 GWd/MTU**
Gap	**Gap**	**Gap**	**Gap**
Typically <1%	Typically <6% to high value of 15%	<5%	<4–5%
Fuel body	**Rim and body**	**Fuel body**	**Rim and body**
3–20%	3–26%	4.7–15%	3–26%

for both PWR and BWR fuels. Similarly, FGRs for higher burnup (>45 GWd/MTU) were typically less than 6 percent with isolated cases with releases up to 15 percent. The graph presented by McKinnon and Cunningham (2003) may represent a bounding case at 60 GWd/MTU and a conservative upper limit of 15 percent could be chosen.

In the absence of data on fission gas releases due to severe impacts and pellet fracturing, data from reactivity-initiated accident transient tests were reviewed in this section (Nuclear Energy Agency, 2010; Beyer and Clifford, 2011) to select proxy FGR values from the rim (and inner core) region in the fuel. Although data on the degree of fracturing or the equivalence of energy imparted between reactivity-initiated accident tests and a 9-m [30-ft] drop impact were not available, it is anticipated that the measured releases of fission gases at grain boundaries and pores in these tests resulted from significant fracturing of the rim (and potentially the inner core) of the fuel. The data examined indicate that high transient FGR values for releases from grain boundaries ranged from 3 to 15 for low-burnup BWR fuel and from 3 to 20 percent for low-burnup PWR fuel. An upper bound of 30 percent is suggested in Table 2-2 for FGR from the grain boundaries and pores from both the rim region and inner core of high-burnup BWR and high-burnup PWR fuels due to severe impacts and pellet fracturing.

4.1.6 Parameter P_{rod}

During reactor operation, the internal pressure in a fuel rod will increase from the initial He gas backfill pressure due to the production and release of fission gases to the gap region. Fission gas production increases with increased burnup. The "end-of-life" pressure in the rod is important for establishing the available gas pressure that could drive particulates from a failed rod into the canister. The pressure in the rod depends on the temperature, which varies along the length of the rod. In most cases, any post-irradiation characterization of rod pressures is done at room temperature and thus pressures would need to be corrected to the average temperature over the rod length in a storage cask. Peak temperatures in a cask could range from 300 to 400 °C [570 to 750 °F] (NRC, 2007). NUREG–1864 (NRC, 2007, Appendix D, p. D–15) estimated that P_{rod} is approximately 5 MPa [50 atm].

New fuel rods are usually backfilled with helium to a pressure of 0.2 to 0.8 MPa [2 to 8 atm] (BWR) and 1–3 MPa [10–30 atm] (PWR) (Nuclear Energy Agency, 2010). Rossiter and Mignanelli (2011) illustrated key parameters for PWR and BWR fuel designs. Typical rod/pin He fill pressures are 2.5 MPa and 1 MPa [25 and 10 atm] for PWR and BWR fuels, respectively. Another concern for gas release from impact could be the release of helium from decay products in the fuel pellet to the plenum, thus increasing the internal rod pressure. Einziger, et al. (1998) calculated the He release after 100 years for a rod with 72 GWd/MTU burnup, assuming a linear production rate with burnup, and found the pressure would increase less than 0.007 MPa [<0.07 atm], which is negligible.

Clarens, et al. (2009) investigated leaching of a PWR fuel with burnups of 48 and 60 GWd/MTU. At a burnup of 60 GWd/MTU the rod had a post-irradiation pressure of 5.9 MPa [58 atm]. The temperature was likely room temperature during the characterization. Rashid and Machiels (2007) presented end-of-life PWR rod internal pressures for 14 × 14 to 17 × 17 rod assemblies with a burnup of 30 to 70 GWd/MTU. There was no obvious increase in pressure with burnup from 30 to 70 GWd/MTU. The mean initial pressures ranged from 2 to 3.45 MPa [20–34 atm]. End-of-life internal pressures ranged from ~2.8 to 4.5 MPa [~28 to 44 atm] and were likely measured at 25 °C [77 °F].

Lanning and Beyer (2004) showed nonproprietary fill-gas pressure for PWR fuels of 2.6–3.3 MPa [26–33 atm]. End-of-life pressures ranged from 10.2 to 12.5 MPa [101 to 123 atm] at 570 °C [1,060 °F] or fuels with burnup <45 GWd/MTU. Principal observations from a post storage examination of low-burnup (23 to 35 GWd/MTU) PWR fuels from a CASTOR–V/21 dry storage demonstration (McKinnon and Cunningham, 2003) indicated that the post storage gas pressure were 3.4 to 3.6 MPa [34 to 36 atm] at 570 °C [1,060 °F] with FGR from 0.4 to 1.0 percent.

Massih, et al. (2005) investigated PCI in BWR and PWR fuels during power ramps. A segmented BWR test fuel assembly was pre-irradiated to 34 GWd/MTU and a short test rod disassembled for the power ramp test. The initial He pressure was 0.4 MPa [4 atm] and FGR was calculated to be 0.3 percent. After the power ramp test, a destructive examination indicated that fractures in the fuel had released 30 percent Xe and that the pin pressure had increased to 2.12 MPa [20.9 atm]. In a second test, a segmented PWR fuel was pre-irradiated to 26 GWd/MTU and a short test rod disassembled for the ramp test. The initial He pressure was 2.5 MPa [25 atm] and FGR was calculated to be 0.1 percent. After the power ramp test, a destructive examination indicated that fractures in the fuel had released 3 percent Xe and that the pin pressure had increased to 3.2 MPa [32 atm].

The Nuclear Energy Agency (2010) reviewed reactivity-initiated accident data and summarized gas pressure in Nuclear Safety Research Reactor tests on pre-irradiated PWR rods. Rod burnup ranged from 39 to 50 GWd/MTU and fill gas pressures before testing ranged from 0.1 to 5.1 MPa [1 to 50 atm]. The measured transient FGR for the rods ranged from 3.5 to 22.7 percent, which contributed to a transient pressure increase in the rod from 3 to 8 MPa [30 to 79 atm].

Rothman (1984) discussed pressures and stresses in PWR and BWR fuel pins applicable to fuel disposal in a tuff host rock repository. A maximum fuel burnup of 38 MWd/MTU was assumed. Various estimates of end-of-life rod pressures at 25 °C [77 °F] ranged from 1.4 to 5.8 MPa [14 to 57 atm] for PWR fuels and 1.4 to 2 MPa [14 to 20 atm] for BWR fuels. The highest pressures, 5.8 and 2 MPa [57 and 20 atm] would give rod pressures of 11 MPa [110 atm] and 4 MPa [40 atm] at 325 °C [617 °F].

Johnson and Gilbert (1983) presented end-of-life internal gas pressure data on PWR and BWR fuels. The pressures were calculated using the GAPCON–Thermal–2 code. The predictions for various burnups for PWR and BWR fuels are shown in Figures 4-4 and 4-5. Johnson quoted end-of-life pressure ranges for “early low-burnup” and “fuels since late 1970s.” Pressures for PWR fuels ranged from 2.5 to 3.5 MPa [25 to 35 atm] for “early” fuels and 3 to 8.1 MPa [30 to 80 atm] for “later” fuels. Similarly, pressures for BWR fuels ranged from 2 to 3.5 MPa [20 to 35 atm] for “early” and 2 to 4 MPa [20 to 40 atm] for “later” fuels. From Figures 4-4 and 4-5, the plenum gas could be as high as 15 MPa [150 atm] at 300 °C [572 °F] for PWR fuel with a burnup of 50 GWd/MTU and as high as 8 MPa [80 atm] at 300 °C [572 °F] for BWR fuel with a burnup of 50 GWd/MTU. These cases represent 20 percent FGR to the gap and pre-pressurization to 3.44 MPa [34.0 atm] and 0.5 MPa [5 atm] for the PWR and BWR fuels, respectively.

Hayes, et al. (1999) present illustrative PWR fill gas pressures from 2 to 4 MPa [20 to 40 atm] at standard temperature and pressure. They also indicate the upper limit for internal operating pressure for fuel rods is approximately 15.5 MPa [153 atm] as the internal pressure is not allowed to exceed the reactor pressure. In a NRC report, NUREG/CR–7001 (Geelhood, et al. 2009) on sensitivity and predictive bias of NRC fuel performance codes, PWR 17 × 17 and

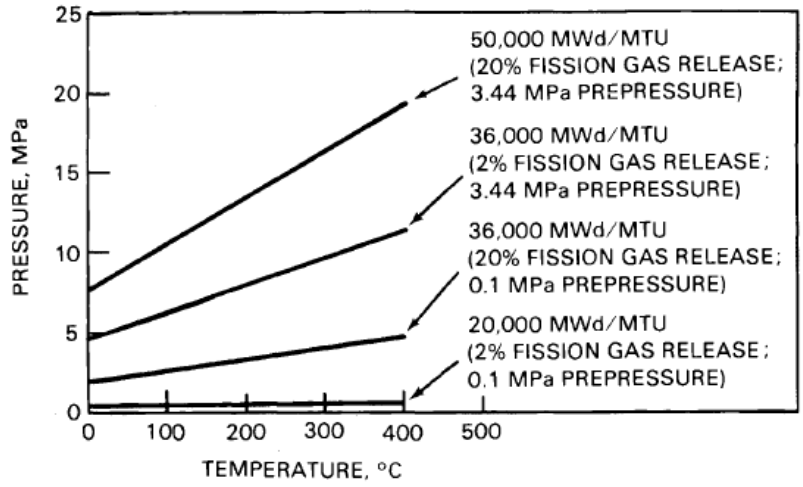

Figure 4-4. Plenum Gas Pressure for Pressurized Water Reactor Spent Fuel Computed From Measured End-of-Life Void Volumes and Indicated Fission Gas Release Assumptions. Pressure/Temperature Relationship From GAPCON–2 (Johnson and Gilbert, 1983, Appendix B).

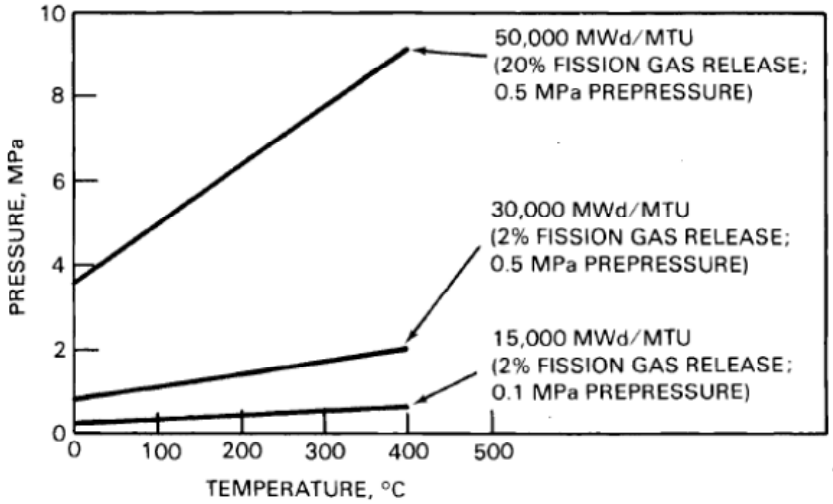

Figure 4-5. Plenum Gas Pressure for Boiling Water Reactor Spent Fuel Computed From Measured End-of-Life Void Volumes and Indicated Fission as Release Assumptions. Pressure/Temperature Relationship From GAPCON–2 (Johnson and Gilbert, 1983, Appendix B).

BWR 10 × 10 coolant pressures of 15.5 and 7.14 MPa [153 and 70 atm] were used as base input for the FRAPCON–3 code based on parameters published in NUREG–1754 (NRC, 2001). These pressures could be considered upper limits for the internal rod pressure.

Kamimura, et al. (2006) examined BWR fuel rod irradiation behavior data (centerline temperature and inner pressure of the fuel rods) using fuel rods equipped with on-line instrumentation. Two rods were irradiated and monitored from insertion up to pellet peak burnup 80 GWd/MTU in the Halden Boiling Heavy Water Reactor. The internal pressure of the

rods increased with burnup. At burnup below 45 GWd/MTU, internal pressures at "hot-standby conditions" were less than 3 MPa [30 atm]. Pressures increased to less than 4 MPa [40 atm] at burnups from 45–60 GWd/MTU and were less than 6 MPa [60 atm] at a burnup of 80 GWd/MTU. Estimated rod pressures based on post-irradiation examination agreed with the measured in-reactor results.

From the literature surveyed, there are cases for which internal rod pressures approach the upper "allowed" limits for the rod pressures of 15.5 and 7.14 MPa [153 and 70 atm] for PWR and BWR SNF, respectively. These upper pressures are limited by the reactor coolant pressure (Geelhood, et al., 2009). For high-burnup fuels, the gap FGR is potentially as high as 15 percent. As fracturing of the rim area for higher burnup fuels could result in release of up to an additional 30 percent of the total fission gas inventory (Section 4.1.5), this would add to the internal pressure in the rod. The results surveyed indicate that end-of-life pressures range from 5 to 15.5 MPa [49 to 153 atm] for high-burnup PWR SNF and 2 to 7.14 MPa [20 to 70 atm] for high-burnup BWR SNF. Given the large variation of internal rod pressures reported in the literature, the ranges of 3 MPa [30 atm] (fill gas pressure) to 15.5 MPa [153 atm] and 1 MPa [10 atm] (fill gas pressure) to 7.14 MPa [70 atm] are representative of low-burnup PWR and low-burnup BWR SNF, respectively. Parameter values suggested for internal rod pressure are tabulated in Tables 2-1 and 2-2.

4.1.7 Parameter A

The leak path area, A is calculated according to Eq. (4-6) as defined in NRC (2007)

$$A = \pi \left(\frac{d_{gap}}{2}\right)^2 \tag{4-6}$$

where d_{gap} is the gap width between the fuel pellet and the clad inner surface. NUREG–1864 (NRC, 2007) estimated A to be 9.6 × 10^{-6} cm^2 for high-burnup BWR fuel with a 35-μm hydraulic diameter. During irradiation, there is a progressive closure of the gap between the fuel pellet and cladding inner surface due to several mechanisms (mainly swelling of the fuel). The gap generally closes with increasing burnup, and ultimately, the fuel and the cladding can contact each other (zero gap). Once contact is established, oxidation of zirconium cladding on the inner surface of the cladding could occur to produce more zirconium oxide as reported for the high-burnup PWR fuel (61 GWd/MTU) by diffusing the oxygen present in the fuel to the cladding side (Lozano, et al., 1998). The thickness of the inner formed zirconium oxide layer was estimated to be 15 μm as determined by electron probe microanalysis. In Dehaudt (2001), the gaps at burnups of 40 and 60 GWd/MTU for PWR fuel are reported to be 14 μm and less than 10 μm, respectively. A similar gap width was also reported of less than 10 μm for high-burnup PWR fuels (Fukeda, et al., 1997). For high-burnup BWR SNF, Nakamura, et al. (2002) indicated the gap can remain open (30 μm). Considering existing information in the literature, leak path dimensions were calculated using Eq. (4-6) for low-burnup PWR SNF and high-burnup PWR and BWR SNF in Table 4-6. No additional information was found for the gap width of low-burnup BWR SNF. Gas-borne flow and filtering of particulates within cladding is assessed in Section 5.1.1.

Table 4-6. Leak Path Dimension (A) for Low- and High-Burnup Pressurized Water Reactor and Boiling Water Reactor SNF [in unit of cm^2]			
Less Than 45 GWd/MTU		**Higher Than 45 GWd/MTU**	
PWR SNF	**BWR SNF**	**PWR SNF**	**BWR SNF**
1.5×10^{-6} (d_{gap} of 14 μm)	No additional information found	0 to 7.9×10^{-7} (d_{gap} of zero to 10 μm)	0 to 7.1×10^{-6} (d_{gap} of zero to 30 μm)
PWR = Pressurized Water Reactor SNF = Spent Nuclear Fuel BWR = Boiling Water Reactor d_{gap} = Gap width between the fuel pellet and the clad inner surface			

4.2 Knowledge Gaps on Fuel Pellet Response

Knowledge gaps associated with fuel pellet responses are as follows:

- Due to the lack of reported data on the fracture behavior of high-burnup fuels under impact loads and the related respirable fraction of the high-burnup fuels, $F_{imp,rim}$, has a large variation, several orders of magnitude. To reduce the range of uncertainty in the current values of $F_{imp,rim}$, better knowledge of the rim fracture size of particulates as a function of impact energy is needed.

- Fracturing and particulate spalling from the fuel pellet rim due to in-reactor cracking after rim development can produce respirable fuel particles as given for $F_{init,rim}$. Bases for parameter value selection are limited due to a lack of published information on rim characteristics.

- The stress induced on the fuel rod by impact can transfer to the fuel pellet and affect the fracture behavior of the fuel pellet. Better understanding of how fuel pellet fracturing depends on the actual energy transferred to the pellet is important for understanding crack propagation and the resultant respirable fractions of the rim and the fuel body. No such analyses were found the literature.

- Fewer data were found for BWR fuels with burnup <45 GWd/MTU. It is anticipated that releases will be similar to or less than PWR fuels in this burnup range. Beyer and Clifford (2011) noted that no FGR measurements exist on the potential transient release associated with fragmentation of high-burnup fuel pellets resulting from an assembly drop or fuel rod balloon/burst and that future testing may be necessary to address the potential transient releases resulting from grain boundary separation and fuel fragmentation.

- The end-of-life rod pressure will be determined by the FGR to the gap, the actual void volume in the rod, and the average rod temperature in the storage cask. In addition, FGR from grain boundaries and pores will add to the fission gas gap release during a drop accident. There are no measurements of transient FGR as a result of drop accidents. Although reactivity-initiated accident tests may provide a good indication of the release of fission gas from grain boundaries and pores, fractures from high temperature excursions may not result in the same gas release as low temperature impact fractures. Uncertainties in the impact fracture properties of the rim in high-burnup

fuels contribute to the lack of knowledge on the total amount of fission gas available for release and internal rod pressure following an impact.

5 AEROSOL DYNAMICS ASSESSMENT

This chapter summarizes the current knowledge on aerosol dynamics for gas and particulate releases from fuel rods within a canister and describes the rationale for parameter value selection. As mentioned in the Introduction, two fuel types (BWR and PWR) and two burnup levels (low and high) are considered.

Following a cladding breach, internal gas pressures within SNF rods represent a driving force for the release of gas and fuel particulates into a SNF canister. Initial and damaged states of SNF, including fuel pellet fracturing, are summarized in Chapter 4. Because the breach sizes and number of breach sites are small compared to the total surface area of cladding (Chapter 3), pathways for the flow of gas and particulates out of SNF rods are confined, and aerosol dynamics considerations are necessary to estimate the extent to which SNF particulates, generated within the fuel rod cladding, can be released from the fuel rods into the canister. Fission product gas and SNF particulates can both contribute to the radiological source term. As mentioned in Chapter 1, activated corrosion products adhering to the outside of SNF cladding (CRUD) were intentionally not considered in this assessment.

Internal gas pressures within SNF rods (NRC, 2007. p. D–15) are significantly greater than pressures within SNF canisters. Accordingly, most of the fission product gas that is available for release will be expelled through one or more breach sites of the fuel rod. A possibility exists for plugging of the flow path with particulate debris prior to fully depressurizing the rod, and this process is investigated in the context of fuel particulate releases. Flow path plugging, however, is not credited in this assessment for reducing the source term of fission product gases because gas migration and seepage through the plug are considered to result in eventual gas releases and contributions to the source term. The challenge in determining the source term for gaseous fission products relates more to quantifying the amount of mobile fission product gas following an event rather than estimating any appreciable retention of mobile fission product gas within breached cladding. For the fuel particulates source term, the challenge lies in both quantifying the amount of respirable-sized particulates generated within the cladding from fuel pellet fracturing or pulverization and the extent to which these particulates can be entrained in the gas flow during rod depressurization and released through a cladding breach. Fuel particulate releases are sensitive to flow characteristics along the leak path within cladding (i.e., Reynolds and Stokes numbers), the pressure differential between the rod and canister, particle plugging within cladding, rod and assembly structures, and canister orientation. Parameters related to aerosol dynamics are introduced in Figure 2-1.

5.1 Existing Knowledge and Selection of Values for Aerosol Dynamics Parameters

This section summarizes the current knowledge on the aerosol dynamics parameters (F_{bed}, $F_{tear,rim}$, $F_{ent,rim}$, and $F_{deposition,k}$). Highlights of literature data are provided in the context of parameter value selection. Recommended parameter values are presented in Tables 2-1 and 2-2.

5.1.1 Parameter F_{bed}

In NRC [2007, Eq. (D.7)], the F_{bed} parameter is defined as the fraction of respirable particles not captured during flow through a particle bed. For high-burnup BWR SNF, a parameter value of 0.1 for F_{bed} can be inferred from NRC (2007, Appendix D, using the equation at the bottom of

page D–9 with the L=10ℓ assignment made at the top of page D–9). Parameter values were not provided in NRC (2007) for high-burnup PWR, lower burnup BWR, or lower burnup PWR SNF. The F_{bed} parameter was reassessed based on relevant literature data. Due to a smaller gap between the fuel rim layer and cladding for high-burnup SNF compared to the gap between the fuel body and cladding low-burnup SNF, the calculation of particle filtering for high-burnup SNF specifically included leak path plugging. Recommended parameter values are presented in Tables 2-1 and 2-2.

Otani, et al. (1989) performed experiments on the filtering efficiency of a particle bed using polystyrene latex (1.04 g cm^{-3}) spherical aerosols. Aerosol particulate diameters ranged from 0.50 to 2.02 μm. Polystyrene latex results were selected for further consideration because the physical diameters and bed packing density for those experiments were more representative of expected conditions for entrainment of SNF particulates inside cladding. The overall filtering efficiency of a 15-cm [5.9-in]-long bed of 1-mm [0.04-in] alumina particles was sensitive to interstitial particulate velocity and aerosol particulate size (Otani, et al., 1989, Figure 4). Gravitational settling is responsible for increased filtration at lower interstitial velocities, and inertial impaction controlled particulate filtration at the higher velocities. The smallest efficiencies corresponded to an intermediate range of interstitial velocities for which neither of those two processes dominated. The lowest particle bed efficiency reported from this set of experiments was 0.2 for smaller-diameter polystyrene latex aerosols. The lowest particle bed efficiency value of 0.2 is overly conservative for the larger expected aerodynamic diameter of SNF particulates with a greater potential for particulate filtering and leak path plugging. Mass particulate flows of Otani, et al. (1989) were not extended into the range to induce large pressure drops or leak path plugging.

Due to their spherical shape and density of 1.04 g cm^{-3}, the polystyrene latex particulate physical diameter is equivalent to its aerodynamic diameter. In contrast, the UO_2 particulates from SNF have a density of 10.96 g cm^{-3} and irregular shapes. Particulates with aerodynamic diameters of 10 μm or less are widely considered as respirable (American Nuclear Society, 1998; Bechtel SAIC Company, LLC, 2007a, Appendix C). For UO_2, an aerodynamic diameter of 10 μm equates to an equivalent volume diameter of approximately 3.16 μm (NRC, 2007, Appendix D, Section 2.5.2) or 3.5 μm (Bechtel SAIC Company, LLC, 2007a, Appendix C). If oxidation were to occur, the particulate density could decrease to 8.35 g cm^{-3} for U_3O_8, and an aerodynamic diameter of 10 μm would equate to an equivalent volume diameter of 4.0 μm for U_3O_8 (Bechtel SAIC Company, LLC, 2007a, Appendix C).

Flow pathways of the Otani, et al. (1989) experiments are considered to be roughly analogous to flow paths for rod depressurization and fuel particulate entrainment within the cladding gap for lower burnup SNF. Because the expected size distribution of SNF particulates is dominated by large, nonrespirable particles (Bechtel SAIC Company, LLC, 2007a, Figure 5) and equivalent volume diameters of SNF particulates relate to even larger aerodynamic diameters, SNF particulates would be more susceptible to filtering compared to the particulate flows of Otani, et al. (1989). For the polystyrene latex particulate flow conditions that are more representative for entrained flow of SNF particulates, the largest filtration efficiencies measured by Otani, et al. (1989) for a bed length of 15 cm [5.9 in] approached, but did not exceed, 95 percent for the overall bed efficiency (Otani, et al. 1989, Figure 4) and less than 0.05 for the single-sphere interception efficiency (Otani, et al. 1989, Figure 13). Sprung, et al. (2000, Section 7.3.3) applied the empirical relationship developed by Otani, et al. (1989, Eq. 13) and calculated bed lengths that would provide 99 percent filtering for different entrained particle sizes and Reynolds numbers. For a 1-foot section of rod of SNF pressurized to 20.5 MPa [202 atm] with a 20 μm gap Sprung, et al. (2000, Section 7.3.3) indicated a calculated He interstitial flow velocity of

1,200 cm s^{-1}. Scoping calculations by Hanson, et al. (2008, Section 4.3) for helium pressurized at 21 MPa [210 atm; 3,000 psi gauge] indicate gas flows greater than 30,000 cm s^{-1} [300 m s^{-1}]. These large flow velocities justify selection of the highest bed filtering efficiencies for polystyrene latex particulates measured by Otani, et al. (1989, Figure 4). The higher flow velocities calculated by Sprung, et al. (2000, Section 7.3.3) were beyond the range included in the Otani, et al. (1989) experiments. Considering uncertainties in the flow regime, Reynolds and Stokes numbers, and flow velocities (NRC, 2007, Appendix D, Section 2.3.2), the particulate filtering efficiency (i.e., greater particulate passage) was not extrapolated beyond the range of measured values for a bed length of 15 cm [5.9 in] so that resulting (F_{bed} parameter) estimates for particulates flowing through the particle bed for a breached rod would not be underestimated. Particulate filtration efficiency was selected to range from 0.86 to 0.94 per 15-cm-long [5.9-in-long]-particle bed length, corresponding to the measured values for 1.10-µm polystyrene latex particulates with an interstitial flow velocity exceeding 200 cm s^{-1} and for 2.02-µm polystyrene latex particulates with an interstitial flow velocity exceeding 100 cm s^{-1}, respectively, from Otani, et al. (1989, Figure 4). No credit for filtering is applied to SNF particulates located 7.5 cm [3.0 in] away from the cladding breach, which is an assumption between the two values used by Sprung, et al. (2000, p. 7-34) for rod breaches not subject to impacts {15.24 cm [6.0 in] in each direction} and subjected to impact fracturing {0.3 cm [0.1 in] in each direction}.

The breach is located at the center axial position of the first 15-cm [5.9-in] segment. No filtering is applied to this rod segment, and its contribution is captured by the F_{tear} parameter in Tables 2-1 and 2-2. The second 15-cm [5.9-in] segment has a center axial position 22.5 cm [8.86 in] away from the breach location; one bed length of filtration is applied to this segment. The third 15-cm [5.9-in] segment has a center axial position 37.5 cm [14.8 in] away from the breach location; two bed lengths of filtration are applied to this segment. Additional rod segments and filtering are applied until the full length of the rod is accounted for. For breaches near the center of a 3.65-m [12-ft]-long rod, F_{bed} is calculated for filtration efficiencies of 0.86 and 0.94 (passage efficiencies of 0.14 and 0.06). Twelve 15-cm [5.9-in] segments on each side of the first 15-cm [5.9-in] segment sum to a length of 375 cm [12.3 ft], which exceeds the 365-cm [12-ft] rod length. As previously described, the F_{bed} parameter does not include contributions near the cladding breach that do not experience filtering by the particle bed.

Center breach, Filtration efficiency for 15-cm [5.9-in] bed length = 0.86, Passage efficiency = 0.14

$$\mathrm{F_{bed}} = 2\left(\frac{7.5}{365}\right)[2(0.14) + 2(0.14)^2 + 2(0.14)^3 + 2(0.14)^4 + \cdots + 2(0.14)^{12}] = 0.01$$

Center breach, Filtration efficiency for 15-cm [5.9-in] bed length = 0.94, Passage efficiency = 0.06

$$\mathrm{F_{bed}} = 2\left(\frac{7.5}{365}\right)[2(0.06) + 2(0.06)^2 + 2(0.06)^3 + 2(0.06)^4 + 2(0.06)^5 + \cdots + 2(0.06)^{12}] = 0.005$$

The F_{bed} values of 0.005 and 0.01 were used to establish a parameter range in Table 2-2 for lower burnup PWR and lower burnup BWR SNF with a cladding breach located at the center of a SNF rod.

For breaches near the end of a 3.65-m [12-ft]-long rod, SNF particulates generated and entrained from the other half of the rod would need to flow through many 15-cm [5.9-in] bed lengths. The same filtration efficiencies of 0.86 and 0.94 are applied to this calculation. The end breach is assumed to be within the first 15-cm [5.9-in] segment from the end of the rod. Twenty-four 15-cm [5.9-in] segments in addition to the first 15-cm [5.9-in] segment sum to a length of 375 cm [12.3 ft], which exceeds the 365-cm [12.3-ft] rod length.

End breach, Filtration efficiency for 15-cm [5.9-in] bed length = 0.86, Passage efficiency = 0.14

$$\mathrm{F_{bed}} = \left(\frac{15}{365}\right)[(0.14) + (0.14)^2 + (0.14)^3 + (0.14)^4 + \cdots + (0.14)^{23} + (0.14)^{24}] = 0.007$$

End breach, Filtration efficiency for 15-cm [5.9-in] bed length = 0.94, Passage efficiency = 0.06

$$\mathrm{F_{bed}} = \left(\frac{15}{365}\right)[(0.06) + (0.06)^2 + (0.06)^3 + (0.06)^4 + (0.06)^5 + \cdots + (0.06)^{23} + (0.06)^{24}] = 0.003$$

The F_{bed} values of 0.003 and 0.007 were used to establish a parameter range in Table 2-2 for lower burnup PWR and lower burnup BWR SNF with a cladding breach located at the end of a SNF rod. This application of measurement data from Otani, et al. (1989) for center and end breaches of SNF focused on particulate filtering. Leak path plugging was not considered. Although a different approach was taken in this calculation, it produced filtering results that agree well with the 1 percent used by Sprung, et al. (2000, Section 7.3.3) for calculating the release fraction of SNF particulates.

For higher burnup fuel, a smaller gap is expected due to the formation of a friable rim. At room temperature, the gap is expected to range from approximately 50 μm to no gap (NRC, 2007, Appendix D, p. D–5). Due to the smaller hydraulic diameters and small to no gap for higher burnup SNF, leak path plugging is considered. Experiments on aerosol plugging in ducts by Morewitz (1982) resulted in an empirical relationship for the total mass of aerosol passed through a round duct of various diameters prior to plugging. Duct diameters ranged from tens of micrometers to tens of centimeters. Experimental results were reported for uranium dioxide, sodium oxides, sodium carbonates, and other aerosol compositions (e.g., Vaughan 1978; Sutter, et al. 1980; Morewitz 1982). In particular, some tests with depleted UO_2 powder (Sutter, et al., 1980) were conducted with pressure differentials of 0.2 and 0.68 MPa [2.0 and 6.7 atm], which are significantly lower than the pressure differential for rod depressurization into the canister. Powers (2009, p. 14) noted that the empirical relationship by Morewitz (1982) and Vaughan (1978) is appropriate when Stokes numbers are large and settling velocities are significant in comparison to aerosol flow velocities. For the expected size distribution of fuel particulates created due to burst releases and impact fracturing, mass median diameters ranging from 150 to about 11,000 μm (Bechtel SAIC Company, LLC, 2007a, Figure 5; Mecham, et al., 1981, Table 2), settling velocities for a majority of the particulate mass will be large (roughly 1 m s^{-1} or greater). The maximum particle size of 11,000 μm in Mecham, et al. (1981, Table 2) is used as the upper bound rather than the larger 18,000-μm statistical value for the computed mass median diameter because it exceeds the size of unfractured pellets {13.7-mm [0.539-in] diameter by 13.6-mm [0.535-in] length} due to a departure from lognormal distribution at large particle sizes.

Bechtel SAIC Company, LLC (2007b, Section 6.3.3.4) compared leak path factors for SNF particulates that escape from a cask to the environment. Leak path factors were calculated using the modeling conventions of Sprung, et al. (2000), Sutter, et al. (1980), and Vaughan (1978) with opening dimensions for cask leakage and pressures up to 0.6 MPa [6 atm or 100 psi

absolute]. Results from this comparison were not used to select parameter values for particulate release from SNF rods, because leakage path areas and pressures are expected to be significantly smaller and larger, respectively, compared to those used in the comparison for leakage from the cask to the environment.

Based on computations presented in Sprung, et al. (2000, Figure 7.10), more than 98 percent of the aerosol particulate mass released from breached SNF into a TN–125 transportation cask had diameters between 0.2 and 20 μm. This particle size range extends slightly beyond the widely accepted maximum physical diameter of 4 to 10 μm for UO_2 particles to be considered as respirable (American Nuclear Society, 1998; Bechtel SAIC Company, LLC, 2007a, Appendix C).

Uncertainties exist with respect to the breach size, Stokes number for fuel rod depressurization, and influence of a greater pressure differential, up to about 5.1 MPa [up to about 50 atm] (NRC, 2007, p. D–15), at the moment that the cladding breaches. Burton, et al. (1993) performed aerosol flow and plugging experiments at pressures of 20–80 kPa [0.2–0.8 atm] with glass microspheres, aerodynamic diameters between 0.7 and 13 μm, in 20-mm [0.79-in]-long capillaries with bores of approximately 30 μm and confirmed the importance of pressure. Burton, et al. (1993) observed a general increase in particulate filtering with increasing time of aerosol flow, increases in particle filtering with decreasing pressure, and leak path plugging at lower pressures. However, experimental conditions of Burton, et al. (1993) included much smaller particulate sizes, pressures, and flow distances than those expected for the SNF case. Additionally, experimental times for aerosol flow ranged from 20 to 120 minutes in Burton, et al. (1993), which are much longer than the very short rod depressurization duration of less than 1 second estimated in a scoping calculation by Hanson, et al. (2008, Section 4.3). Bechtel SAIC Company, LLC (2007a, p. 54) expects the annular flow path in the gap to have an equivalent diameter of less than approximately 0.03 cm [0.01 in] for typical commercial SNF and a high degree of internal deposition for particulate mass that does not originate near the site of the breach. Additional experiments of aerosol transport through leak paths were performed by Morewitz, et al. (1979) for hypothetical core disruptive events in a liquid-metal fast breeder nuclear reactor. These experiments included high concentration UO_2 aerosol flow through a multiple bend leak path including narrow segments and an annular region. Significant particle deposition was observed, and plugging occurred after 5 and 1.5 min for UO_2 particle concentrations of 230 and 900 g m^{-3}, respectively. Morewitz, et al. (1979) commented that turbulent flows of both UO_2 and sodium oxide aerosols at high concentrations quickly formed very large agglomerates. However, these results were not used for determining parameter values in this report because the pressures for these tests were significantly lower than the pressure differential expected for rod depressurization.

To approximate particle plugging effects, an idealized circular duct diameter is calculated for the annular flow of entrained fuel particulates within the cladding gap

$$D_{\text{ideal duct}} = 2\sqrt{t_{\text{gap}}\left(D_{\text{cladding}} - t_{\text{gap}}\right)} \tag{5-1}$$

where, $D_{\text{ideal duct}}$ is the idealized circular duct diameter (cm), t_{gap} is the pellet to cladding gap (cm), and D_{cladding} is the internal diameter of the cladding (cm). Flow geometries are depicted in Figure 5-1. NRC (2007, Section D.2.3.1) pointed out the existing uncertainty with respect to flow contributions through the pellet crack network versus the gap during rod depressurization. No new information was found to address this uncertainty. For this assessment, depressurization and flow in the gap are assumed to dominate over flow within

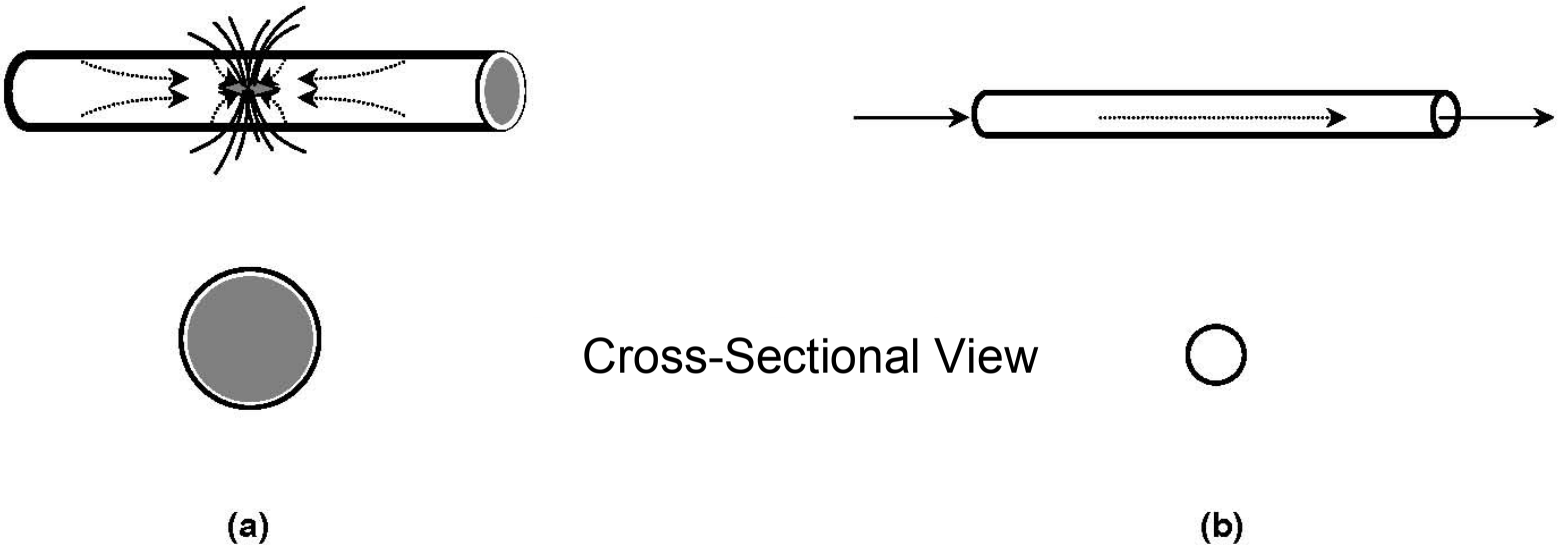

Figure 5-1. Leak Path Geometries for (a) Annular Flow of Gas and Entrained Fuel Particulates Along Fuel Pellet-Cladding Gap and Out Central Breach in Cladding and (b) Idealized Flow Within Circular Duct. Dashed Lines Represent Internal Flow. Solid Lines Represent External Flow.

the crack network. There is a lack of definitive information on the extent to which depressurization through the crack network will influence F_{bed} parameter values. Flow through the gap or portions thereof would still be expected as gas migrates from surrounding areas within the rod toward the cladding breach site. Information on flow path geometries within failed SNF was not found. An idealized circular gap diameter provides a means to assess the F_{bed} parameter. A greater degree of particle filtering and plugging would be expected from irregular (noncircular) flow geometries due to greater surface areas per unit path length and tortuousity compared to a straight circular flow path. If new information indicates flow contributions through the pellet crack network are significant, considerations for the separate treatment of those contributions should be made. For the UO_2 mass within a fuel rod of 2.495 kg [5.5 lb], cladding inner diameter of 0.948 cm, and gap thickness of 0.00825 cm [0.00325 in] {diametrical gap of 0.0165 cm [0.00650 in]} presented in Lorenz, et al. (1980, Section 2.1 and Figure 2), an idealized duct diameter of 0.18 cm [0.46 in] was calculated. For an idealized duct diameter of 0.18 cm [0.46 in], the empirical relationships of Morewitz (1982, Figure 5) and Vaughan (1978, Figure 1) indicate that between 0.03 and 0.10 g of particulate could flow through the cladding gap and escape prior to plugging. Assuming this calculation applies to respirable particulates flowing within the cladding gap, not the mix of primarily larger particles ejected at the site of the cladding rupture, the calculated range for particulate flow and escape represents about 1×10^{-5} to 4×10^{-5} of the total UO_2 mass. Experimental results of Lorenz, et al. (1980), however, indicated a smaller release of respirable particles from fuel rod segments (approximately 2×10^{-6} to 4×10^{-6} for respirable particulates with total release fractions of 2×10^{-4} to 4×10^{-4} for all particles). Application of a circular flow convention and empirical data, to the annular flow case for fuel particulate entrainment and flow within the cladding gap (Figure 5-1), underestimates plugging and overestimates particulate passage and release. Insufficient data are available in the literature to account for previously stated uncertainties on breach size, Stokes number, and pressure differential as well as uncertainties associated with the fracture response and particle size distribution of high-burnup SNF fines generated from impacts. In light of these uncertainties, the anticipated overestimation of particulate passage due to flow path geometry differences is considered to be acceptable for applying published measurement results on particulate flow.

High-burnup fuel with a developed rim structure will have a smaller fuel-cladding gap compared to the previous case using the original gap dimension. For a gap thickness of 0.0025 cm [25-μm], the idealized duct diameter was calculated as 0.097 cm [0.038 in] using Eq. (5-1). For an idealized duct diameter of 0.097 cm [0.038 in], the empirical relationships of Morewitz (1982, Figure 5) and Vaughan (1978, Figure 1) indicate that between 0.007 and 0.015 g of particulate could escape prior to plugging. For the same UO_2 mass in the rod, the released particulate masses equate to 3×10^{-6} to 6×10^{-6} of the total UO_2 mass through the particle filter bed.

Bechtel SAIC Company, LLC (2007a, p.61–62) indicates that a fuel pellet drop from a height of 12 m [39 ft] results in an impact energy density of 1.2 J cm^{-3}. Mecham, et al. (1981, Figures 16 and 17) indicated a mass fraction of about 5×10^{-3} was converted to particles with diameters less than 100 μm due to an impact of 1.2 J cm^{-3} on unclad UO_2 fuel pellets. This fractional conversion of specimen mass to respirable particulate mass is consistent with impact tests on glasses and ceramics for a constant impact energy density of 10 J cm^{-3} (Jardine, et al., 1982, Table 6). Sprung, et al. (2000, pp. 7-32) estimated mass fraction of about 2×10^{-4} to 3×10^{-3} fuel pellet mass converted to respirable particulates for impact velocities ranging between 13 and 54 m s^{-1} [30 and 120 mi] per hour. Sanders, et al. (1992, p. IV–15) concludes that high-burnup fuel yields a higher percentage of fine particles for a given impact energy. This conclusion is associated with much higher impact energies {perhaps two orders of

magnitude higher than those for a 9-m [30-ft] drop} and SNF with burnup of 22 to 33 GWd/MTU, which have not developed a rim structure. By comparing the fractional particulate mass released from cladding prior to plugging to the respirable particulate generated due to impact, the F_{bed} parameter value is recommended to range between 0.015 and 0.03 ($3 \times 10^{-6}/2 \times 10^{-4}$ to $6 \times 10^{-6}/2 \times 10^{-4}$) for high-burnup BWR SNF in Table 2-1. To account for the smaller gap for high-burnup PWR SNF (Table 4-6) and void space for fuel fragments, the F_{bed} value is expected to be smaller than the lower value of 0.015 for high-burnup BWR fuel. Without additional calculations to support selection of a lower value for the greater potential of particulate flow plugging within more confined spaces, a point estimate of 0.01 is suggested for high-burnup PWR SNF in Table 2-2.

Sutter, et al. (1980, Tables A.1 and A.2) performed several hundred experiments using depleted uranium powder, with a mass median diameter of 1 μm and aerodynamic diameter of 3.5 μm, and developed empirical relationships for the amount of aerosol leaked through small openings varying in diameter from 20 to 276 μm. Pressures ranged between 0.03 and 7 MPa [0.3 to 70 atm; 5 and 1,000 psi absolute]. Aperture diameter and pressure were determined to be important parameters. Fuel rod depressurization relates to a high flow case in the Sutter, et al. (1980, Table B33) convention. For the idealized duct diameters above and differential pressures between 10 and 25 atm, the high-flow convention indicated expected leakage of fine (3.5-μm aerodynamic diameter) aerosol would be between about 1 and 11 g for the larger flow dimension of lower burnup fuel and about 0.1 to 0.8 g for the smaller flow path dimensions of higher burnup fuel for a range of flow opening configurations (e.g., orifice type and capillaries) for a large amount of initial aerosol mass. Experiments were performed with initial aerosol masses. Higher pressures increased the calculated aerosol leakage. For pressure increases to 55.1 MPa [50 atm], calculated ranges for leaked mass were determined to increase by a factor of about 2.5 according to the convention. The largest calculated leaked masses were associated with capillaries. Capillary lengths were 0.76 and 2.54 cm. SNF particulates generated from impacts are expected to be considerably larger than the fine particulates used in the Sutter, et al. (1980) experiments. It is expected that SNF particulate generation and entrainment relate to distances to the (closest) rod breach location that are much greater than the capillary lengths of the Sutter, et al. (1980) experiments. Considering the significant differences in particulate size and leak path length, the Sutter, et al. (1980) convention was not used to determine F_{bed} parameter values. However, qualitative consideration of these differences with the ratio of calculated leaked mass to initial aerosol mass suggests that F_{bed} parameter values in Tables 2-1 and 2-2 do not overestimate the amount of particulate filtering and deposition within rod leak paths.

5.1.2 Parameter $F_{tear,rim}$

In NRC [2007, Eq. (D.7)], the $F_{tear,rim}$ parameter is defined as the fraction of UO_2 in the rim layer that is blown out of the rod from one rod tear during rod depressurization without filtering by passage through a particle bed. The $F_{tear,rim}$ parameter in NRC (2007, Eq. D.7) accounts for the localized release of fuel fines originating from rim layer material adjacent to the site of the cladding breach. NRC (2007, Section D.2.4.1.4) and Einziger (2007) suggest a value of 2.8×10^{-4} for the $F_{tear,rim}$ parameter. Alternative estimates to this value were not found in the literature. The $F_{tear,rim}$ parameter value of 2.8×10^{-4} yielded a rod release fraction of respirable particulates from the rim and fuel body of less than 10^{-5} to about 10^{-4} for between 1 and 5 breach sites in a rod due to a 9-m [30-ft] drop (Einziger, 2007, Table 2) assuming a rim entrainment factor of zero to focus on contributions from the localized region of the breach site. These rod release fractions for respirable particulates exceed the experimental values of

2×10^{-6} to 4×10^{-6} in Lorenz, et al. (1980). No new information was found for the $F_{tear,rim}$ parameter. Because SNF with a burnup of less than about 45 GWD/MTU does not form a rim layer, the $F_{tear,rim}$ parameter is not applicable to those SNF categories.

5.1.3 Parameter $F_{ent,rim}$

In NRC [2007, Eq. (D.7)], the $F_{ent,rim}$ parameter is defined as the fraction of UO_2 in the rim layer that is entrained in the depressurization gas flow through the rim layer-cladding gap and transported to the rod tear and then out into the cask. NRC (2007, Section 2.4.1.3) recommends that a $F_{ent,rim}$ parameter of 1 be used unless additional justification is provided to support smaller values. Varying the $F_{ent,rim}$ parameter value between 0 and 1, Einziger (2007, Tables 1 and 2) showed that the release fraction and source term per rod were highly sensitive to the $F_{ent,rim}$ parameter when complete rim fracture was assumed for drops of 0.3 and 9 m [1 and 30 ft]. Beyond considerations given in NRC (2007, Section D.2.4) and Einziger (2007) for the $F_{ent,rim}$ and $F_{tear,rim}$ parameters, no additional data were found in the literature on particulate entrainment due to gases flowing around and through the rim layer or the mass of rim material expelled from cladding at the breach site. Considering existing information, a low end of the $F_{ent,rim}$ parameter range is suggested for high-burnup SNF.

As shown in NRC (2007, Eq. D.7), the $F_{ent,rim}$ parameter is applied to the mass of respirable fuel fines within the cladding that originates from the rim layer. A $F_{ent,rim}$ parameter value of 1 implies that all of the respirable fuel fines from the rim layer would be entrained in the gas flow out of the rod. As discussed in greater detail elsewhere in this chapter, the F_{bed} parameter accounts for the retention of respirable fines within the rod due to particle filtering or flow path plugging. If the rim is assumed to fracture in the same manner as the body, Einziger (2007, Tables 1 and 2) showed that the release fraction or source term per rod would not increase significantly for rim entrainment increases from 0 to 1. Because the gap is small for high-burnup fuel and approaches zero with increasing burnup, Einziger (2007) suggests that a rim entrainment value closer to zero should be used. Considering this limited information, a value of 0.1 is selected to define the low end for an overall $F_{ent,rim}$ parameter range of 0.1 to 1, as shown in Tables 2-1 and 2-2 for high-burnup SNF. Because SNF with a burnup of less than about 45 GWD/MTU does not form a rim layer, the $F_{ent,rim}$ parameter is not applicable to those SNF categories.

5.1.4 Parameter $F_{deposition,k}$

In NRC [2007, Eq. (D.13)], the $F_{deposition,k}$ parameter is defined as the fraction of the materials in chemical element group k that is deposited onto cask interior surfaces after release to the cask atmosphere from failed rods. NRC (2007, Appendix D, pp. D–18 and D–19) selected 0.9 as the $F_{deposition,k}$ parameter value from a range of 0.9 to 0.984. The parameter value of $F_{deposition,k}$ was reassessed based on existing information. Recommended parameter values are presented in Tables 2-1 and 2-2.

Aerosol leakage from inside a cask to the environment, as a function of particulate size, is informative for estimates of particulate deposition within a canister. Sprung, et al. (2000, Section 7.3.8) reported on the MELCOR computer code computations for the leakage of SNF particulates from a TN–125 transportation cask to the environment. Two leak path areas were considered, 4 and 100 mm^2, for transport out of the cask into the environment. These leak paths dictated the time for cask depressurization, based on a 0.5-MPa [5-atm] cask pressure. Deposition within the cask was significant for all particle sizes. A deposition factor is introduced here to quantify the reduction from the aerosol mass released into the cask to the mass

released to the environment. Deposition factors determined from the results in Sprung, et al. (2000, Figure 7.10) are listed in Table 5-1 for different particulate sizes. The leaked mass expressed as a fraction of total aerosol mass is also presented in Table 5-1. Particulates with diameters between 0.6 and 6 μm were most likely to be released and less susceptible to deposition, especially particles with diameters between 1 and 3 μm. Leaked masses in Table 5-1 sum to 0.021 and 0.303 for the two release cases. As defined in NRC (2007, Appendix D, Eq. D.13), $F_{deposition,k}$ equals 1 minus the mass fraction released. The leaked masses, therefore, imply $F_{deposition,k}$ parameter values of 0.70 to 0.98, respectively, as shown in Table 2-2. A single parameter range is suggested because there is insufficient data for ranges for the four categories of SNF under consideration. These values are considered appropriate for determining the source term because cask pressures are not expected to exceed 5 or 6 atm (NRC, 2007, pp. D–4, D–15, and D–17). As described by NRC (2007, p. D–16), pressure build up in the cask from rod depressurization will be small. The upper portion of the suggested parameter range agrees well with assessments by NRC (2007, Section D.2.5.2.2) and Einziger (2007). The upper portion of the range was derived from modeling results for a 3-mm^2 cask leak area and slower cask depressurization, which provides more time for gravitational settling. The lower portion of the range suggests rapid depressurization through a much larger, 100-mm^2 opening could result in less deposition and a larger contribution to the source term.

Sandoval, et al. (1982) conducted quarter scale experiments on surrogate fuel, depleted uranium oxide with cladding, subjected to high energy explosive forces. A 5 × 5 array of 90-cm [35-in]-long surrogate fuel rods was loaded into a steel and lead cask to represent a three-assembly truck cask for PWR fuel (Sandoval, et al. 1982, Figure 1). The high energy blast disrupted 0.216 kg [0.476 lb] of cladding and depleted uranium oxide and resulted in the

Table 5-1. Deposition Factor for SNF Released Into a Transportation Cask, As Determined From Data Presented in Sprung, et al. (Figure 7.10).* The Deposition Factor Quantifies the Reduction in Aerosol Mass Released From Breached SNF Rods to the Mass Released From the Cask.

Particulate Diameter (μm)	Deposition Factor		Leaked Mass Expressed as a Fraction of Total Aerosol Mass	
	3-mm^2 Leak Area	100-mm^2 Leak Area	3-mm^2 Leak Area	100-mm^2 Leak Area
Less than 0.2	170	250	Less than 10^{-4}	Less than 10^{-4}
0.2–0.3	30	100	0.0002	0.0007
0.3–0.6	10	100	0.0004	0.006
0.6–1	5	70	0.003	0.04
1–2	3	30	0.01	0.1
2–3	3	50	0.006	0.1
3–6	5	130	0.001	0.05
6–10	17	500	0.0002	0.006
10–20	130	4,000	Less than 10^{-4}	0.0003
20–30	1,000	10,000	Less than 10^{-4}	Less than 10^{-4}
30–60	10,000	100,000	Less than 10^{-4}	Less than 10^{-4}
Greater than 60	200,000	Greater than 1,000,000	Less than 10^{-4}	Less than 10^{-4}
		Summation	0.021	0.303

SNF = spent nuclear fuel

*Sprung, J.L., D.J. Ammerman, N.L. Breivik, R.J. Dunkart, F.L.Kanipe, J.A. Koski, G.S. Mills, K.S. Neuhauser, H.D. Radloff, R.F. Weiner, and H.R. Yoshimura. NUREG/CR–6672, "Reexamination of Spent Fuel Shipment Risk Estimates." Vols. 1 and 2. Washington, DC: U.S. Nuclear Regulatory Commission. March 2000.

release of 0.78 ± 0.05 g [0.0017 ± 0.0001 lb] of respirable UO_2 particulates from the cask. Average aerosol concentration in the chamber was monitored over time after detonation (Sandoval, et al. 1982, Figure 4). The peak aerosol concentration of 4 g m^{-3} was recorded 12 seconds after detonation. The concentration dropped to about 0.4 g m^{-3} (factor of 10 overall reduction) and 0.04 g m^{-3} (factor of 100 overall reduction) at 60 and 240 minutes after detonation, respectively. The mass median aerodynamic diameter peaked at approximately 3.5 µm and stabilized to 2.0 µm at 30 minutes after detonation. UO_2 particulates were found to account for 7 percent of the total aerosol mass at 0.2 minutes and about 2 percent for more than 10 minutes after detonation. These data suggest enhanced settling of UO_2 particulates relative to aerosol constituents, presumably due to the greater particle density of UO_2 or possibly particle size. Additionally, Sanders, et al. (1991, Section 4.0) assessed particulate deposition due to diffusion and gravitational settling onto surfaces inside the cavity of a cask. Because particulates within the expected size range of 1 to 10 µm adhere strongly to surfaces to which they become attached, resuspension is assumed to be negligible and is not considered further. Adhesion of settled particulates was not expected to be affected by surface vibration.
A separate experiment conducted with actual SNF (Sandoval, et al. 1982, Table 2, Test #5) and different configuration (Sandoval, et al. 1982, Figure 3) indicated that more volatile fission products, Ru-106 and Cs-137, fractionate into smaller particle sizes relative to U-238 (Sandoval, et al. 1982, Figure 5).

5.2 Knowledge Gaps on Aerosol Dynamics

Additional information is needed on the particle size distribution generated from the fracturing of the rim and fuel body in high-burnup SNF. Particle size distribution is an important factor with respect to particulate entrainment and suspension within gas flow, particle filtering, and leak path plug.

6 AREAS FOR FURTHER RESEARCH

Uncertainty in the overall source term is driven by large uncertainties associated with influential parameters. Knowledge gaps and uncertainties pertaining to individual source term parameters were presented in Chapters 3, 4, and 5. Influential parameters with large uncertainties are highlighted in this chapter. Further research in these areas would reduce uncertainties associated with the source term determination for SNF stored in dry casks for more than 120 years.

- Experimental tests on actual high-burnup SNF specimens or irradiated surrogate materials are needed to determine the fracture behavior of the rim in response to impact loads.

- A suitable failure criterion is needed for high-burnup SNF cladding under impact loading to determine the number of breaches that are large enough to allow the release of particulates.

- Failure probabilities for cladding during extended storage should consider lower decay heat outputs, degradation mechanisms associated with hydrogen-related phenomena, and collective effects over long times (especially for high-burnup fuels).

- Experimental work on particle filtering and plugging with UO_2 or suitable surrogates is needed for the flow geometries, leak path dimensions, particle size distributions, and pressure differentials associated with SNF breaches due to impact loads.

As described in Chapter 1, the release of radioactive material from a canister within the dry storage cask was beyond the scope of this project. Assessments of particulate resuspension from surfaces within the canister and filtering or plugging of leak paths out of the canister could lead to significant reductions in released particulate material.

7 REFERENCES

American Nuclear Society. "American National Standard for Airborne Release Fractions at Non-Reactor Nuclear Facilities." ANSI/ANS–5.10–1998. Reaffirmed Without Changes in 2006. La Grange Park: Illinois: American Nuclear Society. 1998.

Barrett, P.R., H. Foadian, Y.R. Rashid, K.D. Seager, and S.E. Gianoulakis. "Spent Fuel Assembly Source Term Sensitivity Parameters." High Level Radioactive Waste Management: Proceedings of the 14th Annual International Conference, Las Vegas, Nevada, April 26–30, 1993. La Grange Park, Illinois: American Nuclear Society and American Society of Civil Engineers. pp. 886–892. 1993.

Bechtel SAIC Company, LLC. "Release Fractions for Spent Nuclear Fuel and High-Level Waste." 000–00C–MGR0–03400–000–00A. ACC: ENG.20071105.0010. ML090770469. Las Vegas, Nevada: Bechtel SAIC Company, LLC. 2007a.

Bechtel SAIC Company, LLC. "Leak Path Factors for Radionuclide Releases from Breached Confinement Barriers and Confinement Areas." 000–00C–MGR0–01500–000–00A. ACC: ENG.20071018.0002. ML092180418. Las Vegas, Nevada: Bechtel SAIC Company, LLC. 2007b.

Beyer, C.E. and P.M. Clifford. "Update of Gap Release Fractions for Non-LOCA Events Utilizing the Revised ANS 5.4 Standard." PNNL–18212. Rev 1. Richland, Washington: Pacific Northwest National Laboratory. June 2011.

Brach, E.W. "Approval of Interim Staff Guidance Memorandum No. 11, Cladding Considerations for the Transportation and Storage of Spent Fuel, Revision 3." Memorandum (November 17) to Spent Fuel Project Office Staff members, NRC. ML0330230281. Washington, DC: U.S. Nuclear Regulatory Commission. 2003. <www. nrc. govlreading-rmladams.html> (14 December 2011).

Burton, A.C., J.P. Mitchell, and D.A.V. Morton. "The Influence of Pressure on the Penetration of Aerosols Through Fine Capillaries." *Journal of Aerosol Science*. Vol. 24, Supplement 1. pp. S559–S560. 1993.

Clarens, F., E. Gonzalez-Robles, F.J. Gimenez, I. Casas, J. de Pablo, D. Serrano, D. Wegen, J.P. Glatz, and A. Martínez-Esparza. "Effect of Burn-Up and High Burn-Up Structure on Spent Nuclear Fuel Alteration." Special Contract 2 of the Collaboration Agreement 159831—First Phase Results. ENRESA–ITU–UPC: 2005–2007. *Publicación Técnica*. 2009.

Dehaudt, P. "Physical and Chemical State of the Nuclear Spent Fuel After Irridiation." *Synthesis on the Long Term Behavior of the Spent Nuclear Fuel*. Section 5.2. CEA–R–5958(E). Vol. I. Paris, France: Commissariat à l'Énergie Atomique. 2001.

DOE. "Section 4.3.3: Free-Fall Spill and Impaction Stress." *DOE Handbook: Airborne Release Fractions/Rates and Respirable Fractions for Non-Reactor Nuclear Facilities.* DOE–HDBD–3010–94. Washington, DC: U.S. Department of Energy. pp. 4–52. December 1994.

Einziger, R.E. "Source Terms for Spent Fuel Transportation and Storage Cask Evaluation." Proceedings of the 15th International Symposium on the Packaging and Transportation of Radioactive Materials (PATRAM 2007), Miami, Florida, October 21–26, 2007. Deerfield, Illinois: Institute of Nuclear Materials Management. 2007.

Einziger, R.E. and C.E. Beyer. "Characteristics and Behavior of High-Burnup Fuel That May Affect the Source Terms for Cask Accidents." *Nuclear Technology.* Vol. 159, No. 2. pp. 134–146. 2007.

Einziger, R.E, M.A. McKinnon, and A.J. Machiels. "Extending Dry Storage of Spent LWR Fuel for Up To 100 Years." Proceedings of the International Symposium on Storage of Spent Nuclear Fuel from Power Reactors, Vienna, Austria, November 9–13, 1998. Vienna, Austria: International Atomic Energy Agency. 1998.

EPRI. "Spent Fuel Transportation Applications—Assessment of Cladding Performance A Synthesis Report." 1015048. Palo Alto, California: Electric Power Research Institute. 2007.

EPRI. "Spent-Fuel Transportation Applications: Modeling of Spent-Fuel Rod Transverse Tearing and Rod Breakage Resulting from Transportation Accident." 1013447. Palo Alto, California: Electric Power Research Institute. 2006a.

EPRI. "Spent Fuel Transportation Applications: Longitudinal Tearing Resulting from Transportation Accidents—A Probabilistic Treatment." 1013448. Palo Alto, California: Electric Power Research Institute. 2006b.

EPRI. "Spent Fuel Transportation Applications: Global Forces Acting on Spent Fuel Rods and Deformation Patterns Resulting from Transportation Accident." 101817. Palo Alto, California: Electric Power Research Institute. 2005a.

EPRI. "Spent Fuel Transportation Applications: Fuel Rod Failure Evaluation Under Simulated Cask Side Drop Conditions." 1009929. Palo Alto, California: Electric Power Research Institute. 2005b.

EPRI. "Failure Criteria for Zircaloy Cladding Using a Damage-Based Metal/Hydride Mixture Model." 1009693. Palo Alto, California: Electric Power Research Institute. 2004.

Fukeda, T., H. Sasajima, Y. Mori, and K. Ishijima. ''Fuel Failure and Fission Gas Release in High-Burnup PWR Fuels Under RIA Conditions.'' *Journal of Nuclear Material.* Vol. 248. pp. 249–256. 1997.

Geelhood, K.J., W.G. Luscher, C.E. Beyer, D.J. Senor, M.E. Cunningham, D.D. Lanning, and H.E. Adkins. NUREG/CR–7001, PNNL–17644, "Predictive Bias and Sensitivity in NRC Fuel Performance Codes." Washington, DC: U.S. Nuclear Regulatory Commission. October 2009.

Hanson, B.D., W. Wu, R.C. Daniel, P.J. MacFarlan, A.M. Casella, R.W. Shimskey, and R.S. Wittman. "Fuel-In-Air FY07 Summary Report." PNNL–17275. Rev. 1. Richland, Washington: Pacific Northwest National Laboratory. September 2008.

Hayes, T.A., R.S. Rosen, and M.E. Kassner. "Critical Analysis of Dry Storage Temperature Limits for Zircaloy-Clad Spent Nuclear Fuel Based on Diffusion Controlled Cavity Growth." UCRL–ID–131098. Livermore, California: Lawrence Livermore National Laboratory. December 1999.

Hirano, Y., Y. Muzumi, K. Kamimura, and Y. Tsukuda. "Irradiation Characteristics of BWR High-Burnup 9 × 9 Lead Use Assemblies." Proceedings of the 2005 Water Reactor Fuel Performance Meeting, Kyoto, Japan, October 2–6, 2005. Tokyo, Japan: Atomic Energy Society of Japan, the European Nuclear Society and the American Nuclear Society. 2005.

IAEA. "Impact of High-Burnup Uranium Oxide and Mixed Uranium-Plutonium Oxide Water Reactor Fuel on Spent Fuel Management." Vienna, Austria: International Atomic Energy Agency. 2011.

Jardine, L.J., W.J. Mecham, G.T. Reedy, and M.J. Steindler. "Final Report of Experimental Laboratory-Scale Brittle Fracture Studies of Glasses and Ceramics." ANL–82–39. Argonne, Illinois: Argonne National Laboratory. 1982.

Johnson, A.B. and E.R. Gilbert. "Technical Basis for Storage of Zircaloy-Clad Spent Fuel in Inert Gases." PNL–4835, UC–85. Richland, Washington: Pacific Northwest Laboratory. September 1983.

Johnson, L., I. Günther-Leopold, J. Kobler Waldis, H.P. Linder, J. Low, D. Cui, E. Ekeroth, K. Spahiu, and L.Z. Evins. "Rapid Aqueous Release of Fission Products From High Burn-Up LWR Fuel: Experimental Results and Correlations With Fission Gas Release." *Journal of Nuclear Materials.* Vol. 420. pp. 54–62. 2012.

Johnson, L, C. Ferry, C. Poinssot, and P. Lovera. "Spent Fuel Radionuclide Source-Term Model for Assessing Spent Fuel Performance in Geological Disposal." Part I: Assessment of the Instant Release Fraction. *Journal of Nuclear Materials*. Vol. 346. pp. 56–65. 2005.

Kamimura, J., K. Ohira, K. Okubo, N. Itagaki, and A. Takagi. "High-Burnup Fuel (Pellet Burnup 80 GWd/t) Behavior—Fission Gas Release, Pellet Swelling, Micro-Structure." International Meeting on LWR Fuel Performance—Nuclear Fuel: Addressing the Future, Salamanca, Spain, October 22–26, 2006. *Transactions*. 2006.

Kapoor, K., A. Ahmad, A. Laksminarayana, and G.V.S. Hemanth Rao. "Fracture Properties of Sintered UO_2 Ceramic Pellets With Duplex Microstructure." *Journal of Nuclear Materials*. Vol. 366. pp. 87–98. 2007.

Koo, Y.-H., B.-H. Lee, J.-S. Cheon, and D.-S. Sohn. "Pore Pressure and Swelling in the Rim egion of LWR High-Burnup UO_2 Fuel." *Journal of Nuclear Materials*. Vol. 295. pp. 213–230. 2001.

Lanning, D.D. and C.E. Beyer. "Estimated Maximum Cladding Stresses for Bounding PWR Fuel Rods During Short-Term Operations for Dry Cask Storage." Richland, Washington: Pacific Northwest National Laboratory. January 2004.

Lanning, D.D., C.E. Beyer, and K.J. Geelhood. NUREG/CR–6534, PNNL–11513, "FRAPCON–3 Updates, Including Mixed Oxide Properties." Vol. 4. Washington, DC: U.S. Nuclear Regulatory Commission. May 2005.

Lorenz, R.A., J.L. Collins, A.P. Malinauskas, O.L. Kirkland, and R.L. Towns. NUREG/CR–0722, "Fission Product Release From Highly Irradiated LWR Fuel." Washington, DC: U.S. Nuclear Regulatory Commission. February 1980.

Lozano, N., L. Desgranges, D. Aymes, and J.C. Niepce. "High Magnification SEM Observations for Two Types of Granularity in a High-Burnup PWR Fuel Rim." *Journal of Nuclear Materials*. Vol. 257. pp. 78–87. 1998.

Manzel, R. and C. Walker. "High-Burnup Fuel Microstructure and its Effect on Fuel Rod Performance." Proceedings From the 2003. International Topical Meeting on Light Water Reactor Fuel Performance, Park City, Utah. La Grange Park, Illinois: American Nuclear Society. 2003.

Massih, A.R., L.O. Jernkvist, J.E. Lindback, and G. Zhou. "Analysis of Pellet-Clad Interaction of LWR Fuel Rods During Power Ramps." Proceedings from the 18th International Conference on Structural Mechanics in Reactor Technology (SMiRT 18) Beijing, China, August 7–12, 2005. SMiRT18–C03–3. Raleigh, North Carolina: North Carolina State University, International Association for Structural Mechanics in Reactor Technology. 2005.

Matzke, H. and J. Spino. "Formation of the Rim Structure in High-Burnup Fuel." *Journal of Nuclear Materials.* Vol. 248. pp. 170–179. 1997.

McKinnon, M.A. and M.E. Cunningham. "Dry Storage Demonstration for High-Burnup Spent Nuclear Fuel— Feasibility Study." PNNL–14390. Richland, Washington: Pacific Northwest National Laboratory. 2003.

Mecham, W.J., L.J. Jardine, G.T. Reedy, and M.J. Steindler. "General Statistical Description of the Fracture Particulates Formed by Mechanical Impacts of Brittle Materials." *Industrial & Engineering Chemistry Fundamentals*. Vol. 22. pp. 384–391. 1983.

Mecham, W.J., L.J. Jardine, R.H. Pelto, G.T. Reedy, and M.J. Steindler. "Interim Report of Brittle-Fracture Impact Studies: Development of a Methodology." ANL–81–27. Argonne, Illinois: Argonne National Laboratory. 1981.

Morel, M., P. Melin, and A. Dumont. "Updated Status of In-Reactor Experience of FRAGEMA Fuel Products." Proceedings From the 1994 International Topical Meeting on Light Water Reactor Fuel Performance, West Palm Beach, Florida, April 17–21, 1994. La Grange Park, Illinois: American Nuclear Society. 1994.

Morewitz, H.A. "Leakage of Aerosols from Containment Buildings." *Health Physics*. Vol. 42, No. 2. pp. 195–207. 1982.

Morewitz, H.A., R.P. Johnson, C.T. Nelson, E.U. Vaughan, C.A. Guderjahn, R.K. Hilliard, J.D. McCormack, and A.K. Postma. "Attenuation of Airborne Debris From Liquid-Metal Fast Breeder Reactor Accidents." *Nuclear Technology*. Vol. 46, No. 2. pp. 332–339. 1979.

Nakamura, T., K. Kusagaya, T. Fuketa, and H. Uetsuka. ''High-Burnup BWR Fuel Behavior Under Simulated Reactivity-Initiated Accident Conditions.'' *Nuclear Technology*. Vol. 138. pp. 246–259. 2002.

Noirot, J., L. Desgranges, and J. Lamontagne. "Detailed Characterizations of High Burn-Up Structures in Oxide Fuels." *Journal of Nuclear Materials*. Vol. 372. pp. 318–339. 2008.

NRC. NUREG–1864, "A Pilot Probabilistic Risk Assessment of a Dry Cask Storage System at a Nuclear Power Plant." Washington, DC: U.S. Nuclear Regulatory Commission. March 2007.

NRC. NUREG–1754, "A New Comparative Analysis of LWR Fuel Designs." Washington, DC: U.S. Nuclear Regulatory Commission. December 2001.

Nuclear Energy Agency. "Nuclear Fuel Behaviour Under Reactivity-initiated Accident (RIA) Conditions." NEA No. 6847. NEA/CSNI/R(2010)1. Paris, France: Nuclear Energy Agency. 2010.

Otani, Y., C. Kanaoka, and H. Emi. "Experimental Study of Aerosol Filtration by the Granular Bed Over a Wide Range of Reynolds Numbers." *Aerosol Science and Technology*. Vol. 10. pp. 463–474. 1989.

Papin, J., B. Cazalis, J.M. Frizonnet, J. Desquines, F. Lemoine, V. Georgenthum, F. Lamare, and M. Petit. "Summary and Interpretation of CABRI REP–NA Program." *Nuclear Technology*. Vol. 157, No. 3. pp. 230–250. 2007.

Powers, D.A. "Aerosol Penetration of Leak Pathways—An Examination of the Available Data and Models." SAND2009–1701. Albuquerque, New Mexico: Sandia National Laboratories. April 2009.

Rashid, J. and A. Machiels "Threat of Hydride Re-orientation to Spent Fuel Integrity During Transportation Accidents: Myth or Reality?" Proceedings of the 2007 International LWR Fuel Performance Meeting, San Francisco, California, September 30–October 3, 2007. Paper 1039. La Grange Park, Illinois: American Nuclear Society. 2007.

Rice, R.W., K.R. McKinney, C.CM. Wu, S.W. Freiman, and W.J.M. Donough. "Fracture Energy of Si3N4." *Journal of Materials Science*. Vol. 20, No. 4. pp. 1,392–1,406. 1985.

Rondinella, V. and T. Wiss. "The High-Burnup Structure in Nuclear Fuel." *Materials Today*. Vol. 13, No. 12. pp. 24–32. 2010.

Rossiter, G. and M. Mignanelli. "The Characteristics of LWR Fuel At High-Burnup And Their Relevance to AGR Spent Fuel." *National Nuclear Laboratory.* Vol. 10, No. 10930, Issue 2. 2011.

Rothman, A.J. "Potential Corrosion and Degradation Mechanisms of Zircaloy Cladding on Spent Nuclear Fuel in a Tuff Repository." UCID–20172. Livermore, California: Lawrence Livermore National Laboratory. September 1984.

Sanders, T.L., K.D. Seager, Y.R. Rashid, P.R. Barrett, A.P. Malinauskas, R.E. Einziger, H. Jordan, T.A. Duffey, S.H. Sutherland, and P.C. Reardon. "A Method for Determining the Spent-Fuel Contribution to Transportation Cask Containment Requirements." SAND90–2406. Albuquerque, New Mexico: Sandia National Laboratories. November 1992.

Sanders, T.L., H. Jordan, V. Pasupathi, W.J. Mings, and P.C. Reardon. "A Methodology for Estimating the Residual Contamination Contribution to the Source Term in a Spent Fuel Transport Cask." SAND90–2407. Albuquerque, New Mexico: Sandia National Laboratories. September 1991.

Sandoval, R.P., J.P. Weber, and G.J. Newton. "Safety Assessment of Spent Fuel Transportation in Extreme Environments." *Nuclear and Chemical Waste Management*. Vol. 3. pp. 5–12. 1982.

Singh, J.P., H.J. Leu, R.B. Poeppel, E. Van Voorhees, G.T. Goudey, K. Winsley and D. Shi. "Effect of Silver and Silver Oxide Additions on the Mechanical and Superconducting Properties of YBa2Cu3$O_{7-\delta}$ Superconductors." *Journal of Applied Physics*. Vol. 66. p. 3154. 1989.

Spino, J., J. Cobos-Sabate, and F. Rousseau. "Room-Temperature Microindentation Behaviour of LWR Fuels." Part 1: Fuel Microhardness. *Journal of Nuclear Materials*. Vol. 322. pp. 203–216. 2003.

Sprung, J.L., D.J. Ammerman, N.L. Breivik, R.J. Dukart, F.L. Kanipe, J.A. Koski, G.S. Mills, K.S. Neuhauser, H.D. Radloff, R.F. Weiner, and H.R. Yoshimura. NUREG/CR–6672, SAND2000–0234, "Reexamination of Spent Fuel Shipment Risk Estimates." Vols. 1 and 2. Washington, DC: U.S. Nuclear Regulatory Commission. March 2000.

Sutter, S.L., J.W. Johnson, J. Mishima, P.C. Owzorski, L.C. Schwendiman, and G.B. Long. NUREG/CR–1099, "Depleted Uranium Dioxide Powder Flow Through Very Small Openings." ML20040901.0241. Washington, DC: U.S. Nuclear Regulatory Commission. February 1980.

Une, K., S. Kashibe, and A. Takagi. "Fission Gas Release Behavior From High-Burnup UO_2 Fuels Under Rapid Heating Conditions." *Journal of Nuclear Science and Technology*. Vol. 43, No. 9. pp. 1,161–1,171. 2006.

Vaughan, E.U. "Simple Model for Plugging of Ducts by Aerosol Deposits." *Transactions of the American Nuclear Society*. La Grange Park, Illinois: American Nuclear Society. Vol. 22. pp. 507–508. 1978.

Wagh, A.S., J.P. Singh, and R.B. Poeppel. "Dependence of Ceramic Fracture Properties." *Journal of Materials Science*. Vol. 28. pp. 3,589–3,593. 1993.

Winnubst, A.J., K. Keizer, and A.J. Burggraaf. "Mechanical Properties and Fracture Behavior of ZrO_2-Y_2O_3 Ceramics." *Journal of Materials Science*. Vol. 18. pp. 1,958–1,966. 1983.

Wu, C.L., J. Lee, D.L. Wu, and L.J. Jardine. "Effects of a Potential Drop of a Shipping Cask, a Waste Container, and a Bare Fuel Assembly During Waste-Handling Operations." SAND87–7082. Albuquerque, New Mexico: Sandia National Laboratories. December 1991.

Zimmermann, A., M. Hoffman, B.D. Flinn, R.K. Bordia, T.-J. Chuang, E.R. Fuller and J. Roedel. "Fracture of Alumina With Controlled Pores." *Journal of the American Ceramic Society.* Vol. 81, No. 9. pp. 2,449–2,457. 1998.